# REPORT 954

## TWO-DIMENSIONAL COMPRESSIBLE FLOW IN CENTRIFUGAL COMPRESSORS WITH STRAIGHT BLADES

By John D. Stanitz and Gaylord O. Ellis


### SUMMARY

*Six numerical examples are presented for steady, two-dimensional, compressible, nonviscous flow in centrifugal compressors with thin straight blades, the center lines of which generate the surface of a right circular cone when rotated about the axis of the compressor. A seventh example is presented for incompressible flow. The solutions were obtained in a region of the compressors, including the impeller tip, that was considered to be unaffected by diffuser vanes or by the impeller-inlet configuration. Each solution applies to radial- and mixed-flow compressors with various cone angles but with the same angle between blades on the conic flow surface. (The solutions also apply to radial- and mixed-flow turbines with the rotation and the flow direction reversed.) The effects of variations in the following parameters were investigated: (1) flow rate, (2) impeller-tip speed, (3) variation of passage height with radius, and (4) angle between blades on conic flow surface. The numerical results are presented in plots of the streamlines and constant Mach number lines.*

*Correlation equations are developed whereby the flow conditions in any impeller with straight blades can be determined (in the region investigated by this analysis) for all operating conditions. As examples of the information provided by the correlation equations, the velocities along the blade surfaces are presented for a wide range of impeller-tip Mach number, flow coefficient (flow rate), and angle between blades on the conic flow surface.*


### INTRODUCTION

At the present time, the design of centrifugal compressors is primarily an art rather than a science. Little detailed knowledge of flow conditions within the compressor on which to base a rational design is available. If these flow conditions could be determined, design methods might be developed for centrifugal compressors with higher aerodynamic efficiency and better over-all performance. For example, the compressor efficiency would be improved if favorable velocity distributions (with respect to boundary-layer growth and separation) could be obtained along the flow surfaces by proper design of the compressor.

For a given set of design and operating parameters, the velocities and pressures within the compressor depend on the three-dimensional flow path and on the fluid properties (compressiblity and viscosity). A complete analysis of the flow must include all these factors. If flow conditions are essentially uniform in one direction, however, the flow is adequately represented by a two-dimensional analysis in which the fluid is considered inviscid but compressible. Viscosity of the fluid is unimportant except within the boundary layer along the flow surfaces, and this boundary layer is thin provided favorable velocity distributions exist within the compressor. On the other hand, compressibility of the fluid is important in centrifugal compressors because the large pressure ratios per stage result in density changes that affect fluid velocities, streamlines, and so forth.

In a previous report (reference 1), a general method of analysis is developed for steady, two-dimensional, compressible flow through radial- and mixed-flow compressors and turbines in which the center line of the passage generates the surface of a right circular cone when rotated about the axis of the machine. The two-dimensional flow pattern is considered to lie upon the surface of this cone.

In the present report, these analytical methods are applied to investigate the flow conditions within a certain region of radial- or mixed-flow compressors (and turbines) with thin straight blades lying on conic radii (elements). The region investigated includes the impeller tip and is that region considered to be unaffected by the inlet configuration of the impeller and by the diffuser vanes; that is, the impeller inlet and the diffuser vanes (if any) must be far enough removed from the region investigated not to affect the flow appreciably in that region. Straight blades were selected because they were considered the most representative blade shape now in use for aircraft centrifugal compressors.

The purpose of this analysis was to determine the effect of operating and design variables (impeller-tip speed, compressor flow rate, variation of passage height with radius, and angle between blades on conic flow surface) on flow conditions within the region investigated. From this information, limitations can be placed on the operating and design variables if certain flow conditions are desired within these regions. For example, if from boundary-layer considerations maximum rates of deceleration of the relative velocity are specified along the flow surfaces, the results of this analysis can be used to determine limiting values of impeller-tip speed, compressor flow rate, variation of passage height with radius, and angle between blades on conic flow surface.

The theoretical investigation presented herein was conducted at the NACA Lewis laboratory during 1948.

## METHOD OF SOLUTION

### EQUATIONS

A general analysis is developed in reference 1 for steady, two-dimensional, compressible flow in compressors and turbines with arbitrary blade shapes and arbitrary variations in the passage height. The analysis is limited to radial- and mixed-flow compressors and turbines in which the center line of the passage generates the surface of a right circular cone when rotated about the axis of the machine (fig. 1).

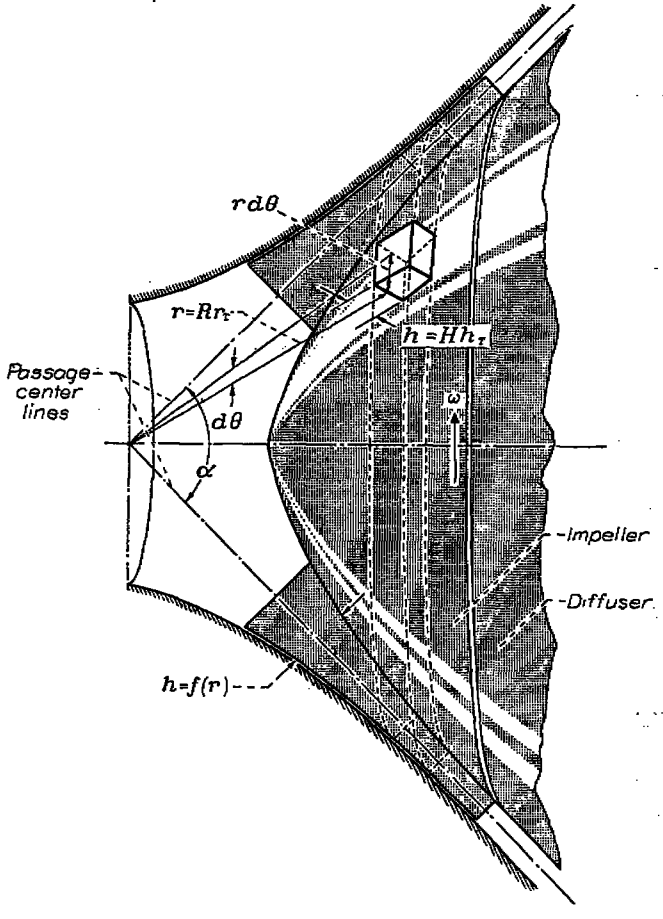


FIGURE 1.—Fluid particle on rotating coordinate system of impeller. Center line of flow passage generates surface of right circular cone with cone angle $\alpha$.

The two-dimensional flow pattern is considered to lie on the surface of this cone. The method of analysis is applied herein to radial- or mixed-flow compressors with thin straight blades lying on conic radii (elements). The equations developed in reference 1 are presented in this section with a brief discussion of the coordinate system and the assumptions and the limitations of the analysis.

**Coordinate system.**—A developed view of the conic flow surface generated by the passage center line (fig. 1) is shown in figure 2. The dimensionless conic coordinates of a fluid particle on the conic flow surface are $R$ and $\theta$. (All symbols are defined in appendix A.) The coordinate $\theta$ is considered

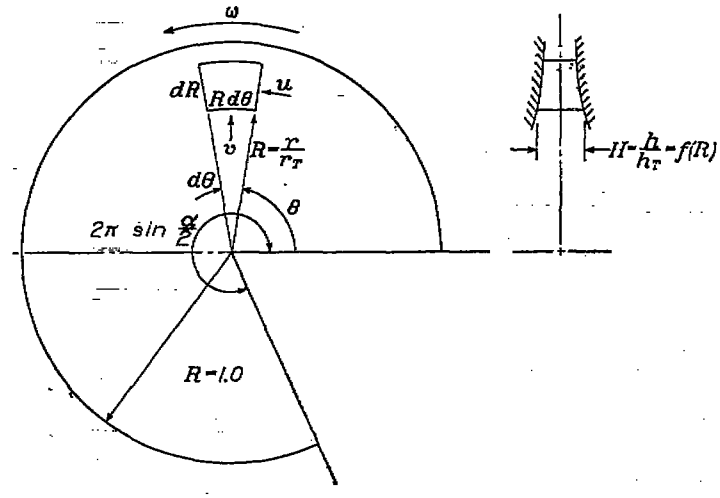


FIGURE 2.—Fluid particle on developed view of conic surface. Dimensionless coordinates relative to impeller $R$, $\theta$, and $H$; tangential and radial components of velocity relative to impeller $u$ and $v$, respectively.

positive in the counterclockwise direction. The conic-radius ratio $R$ is defined by

$$R=\frac{r}{r_T} \tag{1}$$

where $r$ is the conic radius (distance along conic element from apex of cone) and the subscript $T$ refers to the impeller tip. The coordinate system $(R,\theta)$ rotates in the positive direction of $\theta$ with the angular velocity $\omega$ of the impeller. The passage-height ratio $H$, in the direction normal to the conic flow surface (fig. 2), is a continuous function of the conic-radius ratio $R$.

$$H=\frac{h}{h_T}=f(R) \tag{2}$$

where $h$ is the passage height at any conic-radius ratio $R$.

**Assumptions and limitations.**—This analysis assumes that flow conditions are uniform across the passage normal to the conic flow surface; that is, the flow varies only along the conic flow surface. In order to satisfy this assumption, it is necessary that: (1) the gradient of $h$ with respect to $r$ be small; and (2) the cone angle $\alpha$ be sufficiently close to 180°. The allowable variation in $\alpha$ from 180° will depend on the ratio $h/r$ and on the desired accuracy. For the hypothetical limiting case in which $h/r$ approaches zero everywhere along the conic flow surface, the analysis is accurate for all values of $\alpha$.

**Velocity-ratio components.**—The fluid particle on the developed conic flow surface in figure 2 has a relative tangential-velocity ratio $U$ and a radial- (along conic element) velocity ratio $V$. These velocity ratios are defined by

$$U=\frac{u}{c_o} \tag{3a}$$

and

$$V=\frac{v}{c_o} \tag{3b}$$

where

$u$ tangential component of velocity relative to impeller in positive direction of $\theta$ (fig. 2)

$v$ radial (along conic element) component of velocity (fig. 2)

$c$ local speed of sound

Subscript:

$o$ absolute stagnation condition in region of uniform flow upstream of impeller

**Stream function $\psi$.**—A dimensionless stream function $\psi$ satisfies the continuity equation if defined as

$$\frac{\partial \psi}{\partial \theta}=\frac{\rho}{\rho_o} VHR \tag{4a}$$

and

$$\frac{\partial \psi}{\partial R}=-\frac{\rho}{\rho_o} UH \tag{4b}$$

where $\rho$ is the weight density.

The stream function $\psi$ is constant along the blade surface. If $\psi$ and $\theta$ are assigned values of zero along the positive blade surface (the blade surface in the positive direction of $\theta$), the value of $\psi$ along the negative blade surface (the blade surface in the negative direction of $\theta$) is given by

$$\psi_n=\varphi \Delta\theta \tag{5}$$

where $\Delta\theta$, the angle between blades on the conic flow surface, is given by

$$\Delta\theta=\frac{2\pi}{B}\sin\frac{\alpha}{2} \tag{6}$$

and where

$$\varphi=\frac{W}{\rho_o a_T c_o} \tag{7}$$

where

$$a_T=B(\Delta\theta) r_T h_T \tag{7a}$$

where

$\varphi$ compressor flow coefficient

$W$ total compressor flow rate

$a$ annular flow area (normal to conic flow surface)

$B$ number of passages (or blades)

Subscript:

$n$ negative blade surface (blade surface in negative direction of $\theta$)

**Differential equation.**—The differential equation for the stream-function distribution in compressors with thin straight blades lying on conic radii (elements) is obtained from equation (14) of reference 1 in terms of transformed coordinates $\xi$ and $\eta$.

$$2M_T\frac{\rho}{\rho_o}(\Delta\theta)^2 exp\,[(m+2)\xi\Delta\theta]=\frac{\partial^2\psi}{\partial\xi^2}+\frac{\partial^2\psi}{\partial\eta^2}-\frac{\partial\psi}{\partial\xi}\frac{\partial\left(\log_e\frac{\rho}{\rho_o}\right)}{\partial\xi}-\frac{\partial\psi}{\partial\eta}\frac{\partial\left(\log_e\frac{\rho}{\rho_o}\right)}{\partial\eta}-m(\Delta\theta)\frac{\partial\psi}{\partial\xi} \tag{8}$$

where the impeller-tip Mach number $M_T$ is defined as

$$M_T=\frac{\omega r_T \sin\frac{\alpha}{2}}{c_o} \tag{9}$$

The transformed coordinates $\xi$ and $\eta$, which for thin straight blades lying on conic radii are related to $R$ and $\theta$ by

$$\xi=\frac{\log_e R}{\Delta\theta} \tag{10a}$$

$$\eta=\frac{\theta}{\Delta\theta} \tag{10b}$$

have been introduced because they result in parallel blades in the transformed plane. Such a transformation is desirable because it simplifies the solution of the differential equation by relaxation methods.

In equation (8), the passage-height ratio $H$ is assumed to vary with the conic-radius ratio according to

$$H=R^m \tag{11}$$

where $m$ is an arbitrary exponent. (For $m=0$, the blade height remains constant and for $m=-1.0$, the flow area normal to the conic flow surface remains constant.)

In order to solve equation (8), it is necessary to know the density ratio, which is related to the impeller-tip Mach number and the relative velocity ratio $Q$ by (equation (11), reference 1)

$$\frac{\rho}{\rho_o}=\left\{1+\frac{\gamma-1}{2}[(RM_T)^2-Q^2]\right\}^{\frac{1}{\gamma-1}} \tag{12}$$

where $\gamma$ is the ratio of specific heats and

$$Q^2=U^2+V^2 \tag{13}$$

and the absolute whirl of the fluid upstream of the impeller is assumed to be zero. The velocity $Q$ (multiplied by $\rho/\rho_o$) is in turn given by equations (4), (10), (11), and (13) as

$$\frac{\rho}{\rho_o}Q=\frac{1}{(\Delta\theta)\,exp\,[(m+1)\xi\Delta\theta]}\left[\left(\frac{\partial\psi}{\partial\xi}\right)^2+\left(\frac{\partial\psi}{\partial\eta}\right)^2\right]^{\frac{1}{2}} \tag{14}$$

Equations (8), (12), and (14) provide three equations with three unknowns $\rho/\rho_o$, $Q$, and $\psi$.

## NUMERICAL PROCEDURE

The system of equations (8), (12), and (14) is solved by relaxation methods to obtain the stream-function distribution within the compressor. From this distribution, the velocity components and other conditions can be determined using equations (4) and so forth. Detailed outlines for the numerical procedure are given in references 1 and 2. The procedure is briefly sketched herein.

**Outline of procedure.**—In order to solve the system of equations by relaxation methods, the following procedure is employed:

(1) Equations (8) and (14) are changed to finite-difference form (to be discussed).

(2) Values of $\psi$ are specified on the boundaries of the flow region.

(3) Values of $\psi$ are estimated at equally spaced points of a grid system within the boundaries of the flow region.

(4) The preceding estimated values of $\psi$ are adjusted (relaxed) by the relaxation process until they satisfy equation (8) in finite-difference form.

(5) The boundary values of $\psi$ in the vaneless diffuser are adjusted to satisfy the Joukowski condition for tangency of flow leaving the tip of the impeller blade.

(6) After the Joukowski condition has been satisfied, the grid spacing is reduced near the impeller tip in order to obtain detailed knowledge of the flow characteristics in this region where conditions are rapidly changing.

**Finite-difference equations.**—Equation (8) is changed to the following finite-difference form (reference 1):

$$\psi_1+\psi_2+\psi_3+\psi_4-4\psi-\frac{(\psi_1-\psi_3)}{4}\left(\log_e\frac{\rho_1}{\rho_0}-\log_e\frac{\rho_3}{\rho_0}\right)-\frac{(\psi_2-\psi_4)}{4}\left(\log_e\frac{\rho_2}{\rho_0}-\log_e\frac{\rho_4}{\rho_0}\right)-\frac{mb}{2}(\Delta\theta)(\psi_1-\psi_3)-2M_T\frac{\rho}{\rho_0}(\Delta\theta)^2\,exp\,[(m+2)\xi\Delta\theta]\,b^2=\mathrm{R} \qquad (15)$$

where

$b$ grid spacing (fig. 3)

R residual (error) due to estimated values of $\psi$ used during relaxation solution

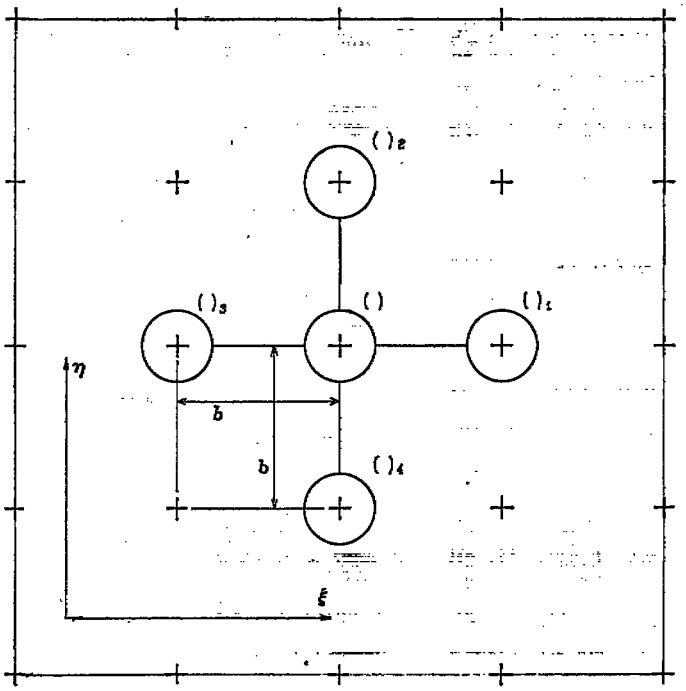


FIGURE 3.—Sample grid showing grid spacing $b$ and numerical subscript convention for adjacent grid points.

Subscripts:

1, 2, 3, and 4 quantities at adjacent grid points as defined in figure 3 (Quantities without numerical subscripts refer to grid point at which R is being computed.)

From equation (12), the natural logarithm of the density ratio (required for the solution of equation (15)) is plotted as a function of the flow-rate ratio $Q\rho/\rho_0$ in figure 4. The flow-rate ratio is obtained from equation (14), which in finite-difference form becomes

$$\frac{\rho}{\rho_0}Q=\frac{[(\psi_1-\psi_3)^2+(\psi_2-\psi_4)^2]^{\frac{1}{2}}}{2b(\Delta\theta)\,exp\,[(m+1)\xi\Delta\theta]} \qquad (16)$$

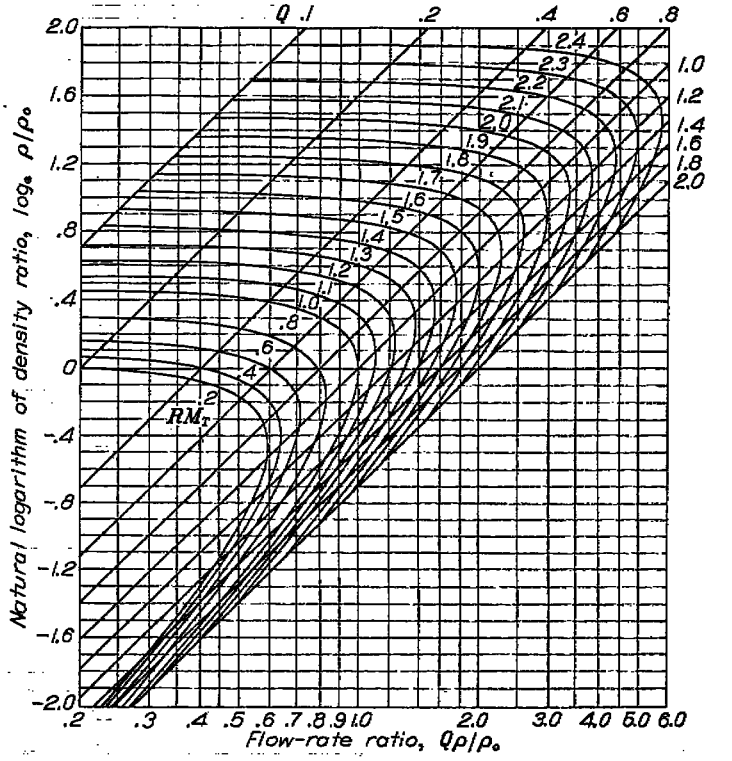


FIGURE 4.—Natural logarithm of density ratio log$_e$ $\rho/\rho_0$ as function of flow-rate ratio $Q\rho/\rho_0$ for various values of $RM_T$. Equation (12); ratio of specific heats $\gamma$, 1.4.

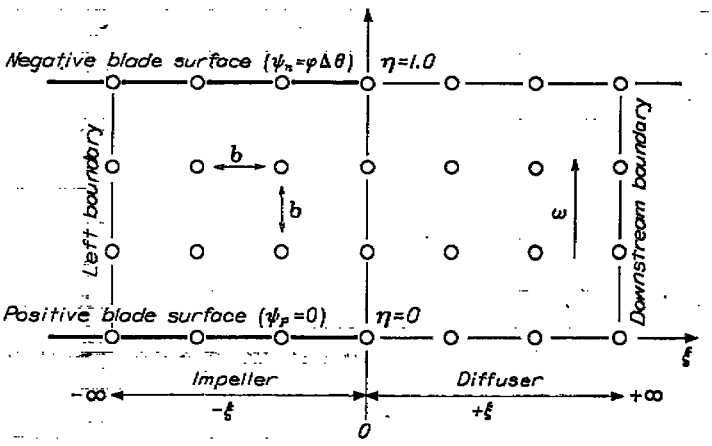


FIGURE 5.—Relaxation grid in plane of transformed coordinates.

**Boundary values of $\psi$.**—The stream function $\psi$ is constant along the blade surfaces. If the value of $\psi$ is arbitrarily set equal to zero along the positive blade surface, the value along the negative blade surface is given by equation (5). Values of $\psi$ along the left boundary (fig. 5) are obtained

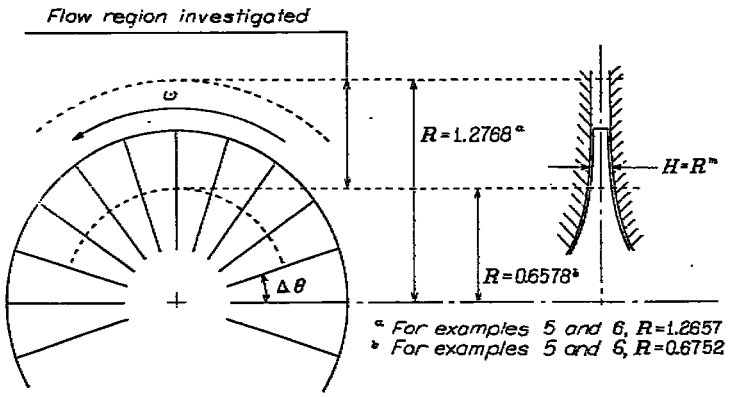


FIGURE 6.—Compressor-design characteristics for numerical examples.

from the simplified analysis of reference 1, which assumes that the flow is parallel to the blade surfaces. Values of $\psi$ along the boundaries of constant $\eta$ in the vaneless diffuser are estimated by a one-dimensional analysis of the flow (reference 1), which assumes the moment of momentum to be constant. (Note that these boundary values of $\psi$ in the diffuser are only approximate and must therefore be relaxed along with the values of $\psi$ at interior grid points, as indicated in reference 1.) At any value of $\xi$ in the vaneless diffuser, the values of $\psi$ along the boundary $\eta=1.0$ are $\psi_n$ greater than the values of $\psi$ along the boundary $\eta=0$. The values of $\psi$ along the downstream boundary of the diffuser (fig. 5) vary linearly.

**Estimated interior values of $\psi$.**—Correlation equations developed in this report (and presented in a later section) provide a first approximation for $\psi$ at grid points within the impeller passage. The error in these estimated values of $\psi$ will, in most cases, be less than $\pm 1$ percent of $\psi_n$.

**Relaxation process.**—The residuals R that result from the estimated interior values of $\psi$ are computed at each grid point by equation (15). These residuals are then reduced (relaxed) by suitable changes in the values of $\psi$. The detailed procedure is given in references 1 and 2.

**Joukowski condition.**—The Joukowski condition requires that the streamline leaving the blade surface be tangent to the blade tip. This condition generally is not satisfied by the initial relaxation solution because for this solution the boundary values of $\psi$ along the downstream boundary in the vaneless diffuser (fig. 5) are obtained from the estimated variation in $\psi$ along the boundaries of constant $\eta$ in the diffuser (discussed in the section **Boundary values of $\psi$**). In order to satisfy the Joukowski condition, the values of $\psi$ along the downstream boundary must all be changed by the same required amount and this change in the boundary values of $\psi$ results in changes in $\psi$ at each of the interior grid points. The manner in which these changes in $\psi$ are made to satisfy the Joukowski condition is discussed in reference 1.

## RESULTS

Seven numerical examples are presented. One of these examples has been selected as the "standard" and in each of the remaining examples one parameter is varied from the standard conditions as shown in the following table:

| Example | $\varphi$ | $M_T$ | $m$ | $\Delta\theta$ (deg) | Type of flow |
|---|---|---|---|---|---|
| Standard | 0.5 | 1.5 | −1.0 | 12 | Compressible ($\gamma$=1.4) |
| 1 | .7 | 1.5 | −1.0 | 12 | Compressible ($\gamma$=1.4) |
| 2 | .9 | 1.5 | −1.0 | 12 | Compressible ($\gamma$=1.4) |
| 3 | .5 | 2.0 | −1.0 | 12 | Compressible ($\gamma$=1.4) |
| 4 | .5 | 1.5 | −1.4 | 12 | Compressible ($\gamma$=1.4) |
| 5 | .5 | 1.5 | −1.0 | 18 | Compressible ($\gamma$=1.4) |
| 6 | .5 | 1.5 | −1.0 | 18 | *Incompressible* |

By comparing the solution for the standard example with one of the nonstandard examples, the effect of the change in a single design or operating parameter on flow conditions in the compressor can be determined.

These examples are for impellers having straight blades (fig. 6). The solutions were obtained in a region of the compressors (including the impeller tip, fig. 6) that was considered to be unaffected by the inlet configuration of the impeller and by the diffuser vanes; that is, the diffuser vanes, if any, must be far enough removed from the impeller not to affect the flow region being investigated. Each solution applies, within the limitations imposed by the assumption of two-dimensional flow, to radial- and mixed-flow compressors (and turbines) with conic flow surfaces having various cone angles $\alpha$ but the same angle between blades on the conic flow surface $\Delta\theta$ (reference 1).

The numerical results are presented in plots of the streamlines and constant Mach number lines.

**Streamlines.**—The streamline configurations (relative to the impeller) for the seven examples are shown in figure 7. The streamlines are designated in such a manner ($\psi/\psi_n$) that the value of a streamline indicates the ratio of the flow that lies between the streamline and the positive blade surface to the total flow in the passage. For a given density ratio, the streamline spacing is indicative of the velocities relative to the impeller, with close spacing indicating high velocities and wide spacing indicating low velocities.

The streamlines for the standard example are given in figure 7 (a). For the design and operating conditions of this example, an eddy has begun to form on the positive blade surface. This eddy results from negative velocities on and near the blade surface. The fluid in this eddy rotates (relative to the impeller) in the opposite direction to that of the impeller so that the absolute motion of the fluid is irrotational. In actual practice this eddy is probably unstable and it is desirable to eliminate the eddy by proper changes in the design and operating conditions of the compressor. From an inspection of figure 7, it appears that the eddy can be reduced or eliminated by increasing the flow coefficient $\varphi$ (figs. 7 (b) and 7 (c)), decreasing the impeller-tip Mach number $M_T$ (fig. 7 (d)), decreasing the angle between blades on the conic flow surface $\Delta\theta$ (fig. 7 (f)), and using incompressible fluids (fig. 7 (g)). The eddy in figure 7 (d) (impeller-tip Mach number of 2.0) is especially interesting because it occupies more than one-half of the available flow area at a radius ratio of 0.90.

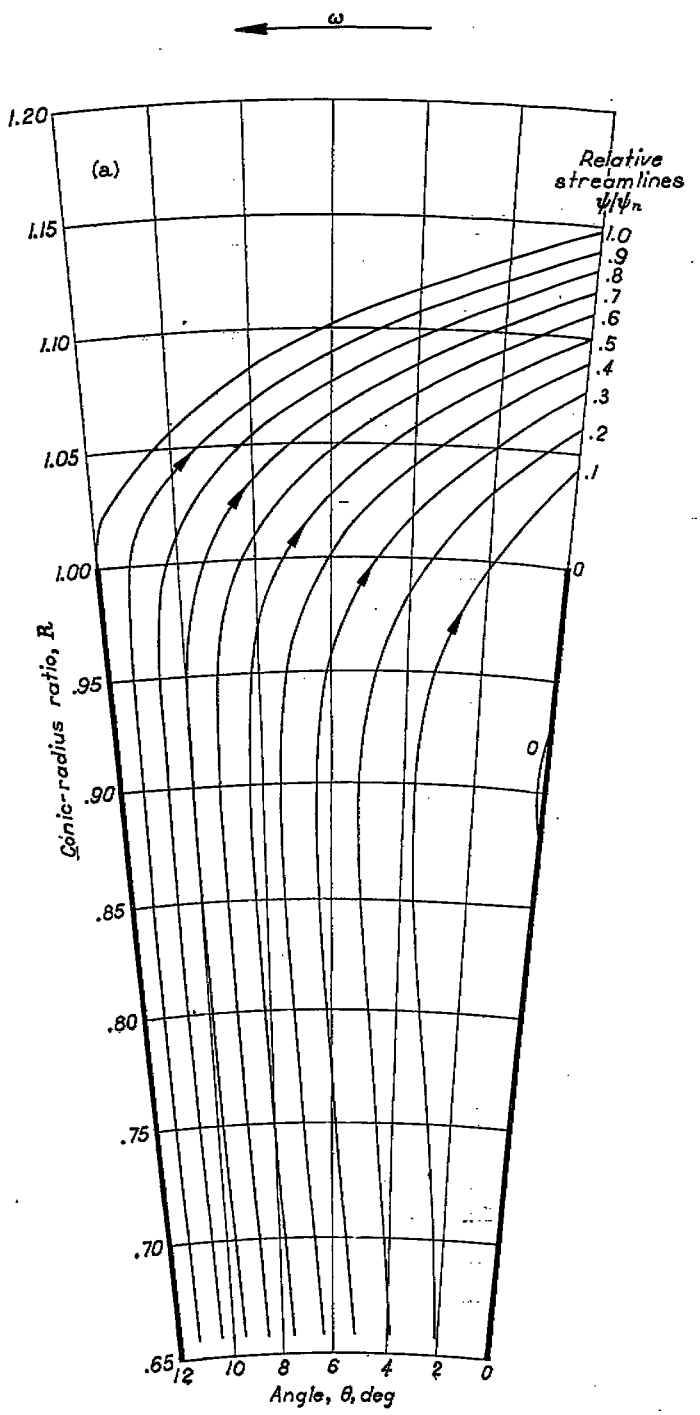


(a) Standard example: flow coefficient $\varphi$, 0.5; impeller-tip Mach number $Mr$, 1.5; constant flow area ($m$, −1.0); angle between blades on conic flow surface $\Delta\theta$, 12°; compressible flow ($\gamma$, 1.4).

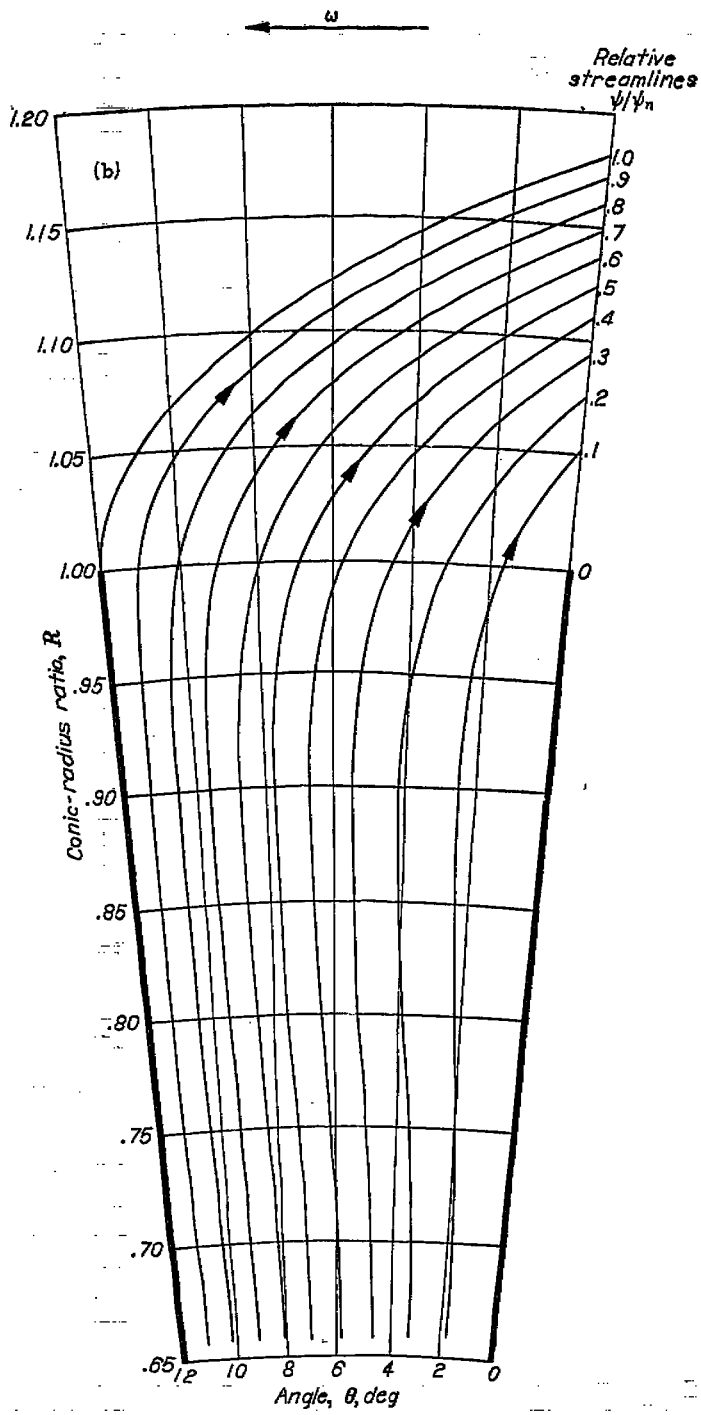


(b) Example 1: flow coefficient $\varphi$, 0.7; other parameters same as standard example.

FIGURE 7.—Relative streamlines for flow through centrifugal compressor with straight blades. Streamline designation indicates ratio of flow that lies between streamline and positive blade surface (right side of passage) to total flow in passage.

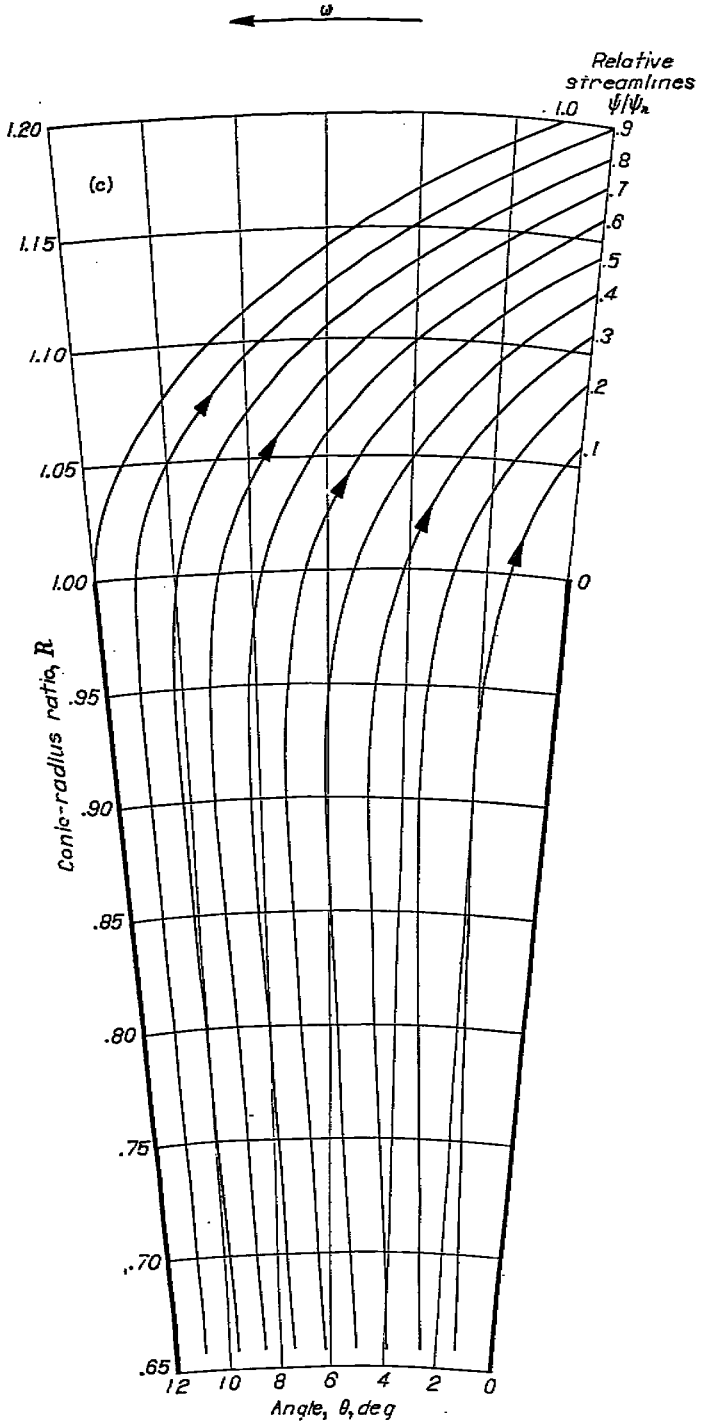


(c) Example 2: flow coefficient $\varphi$, 0.9; other parameters same as standard example.

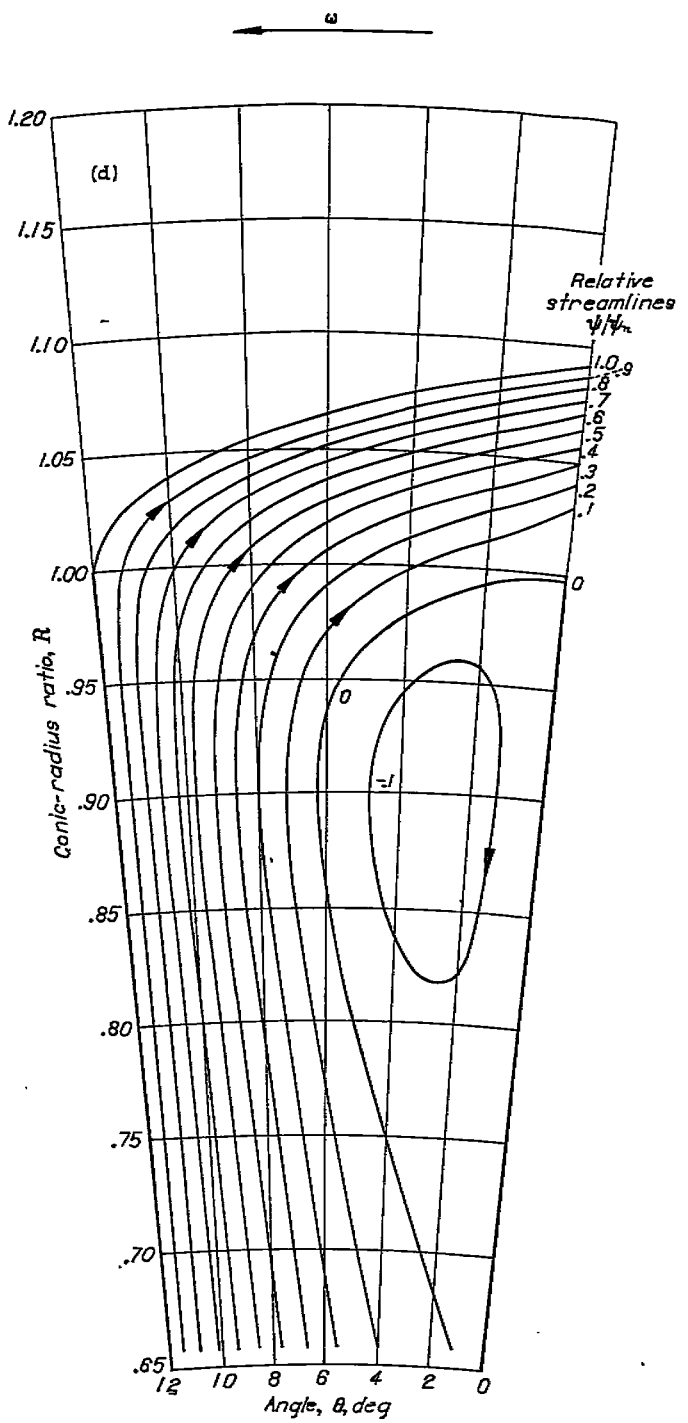


(d) Example 3: impeller-tip Mach number $M_T$, 2.0; other parameters same as standard example.

FIGURE 7.—Continued. Relative streamlines for flow through centrifugal compressor with straight blades. Streamline designation indicates ratio of flow that lies between streamline and positive blade surface (right side of passage) to total flow in passage.

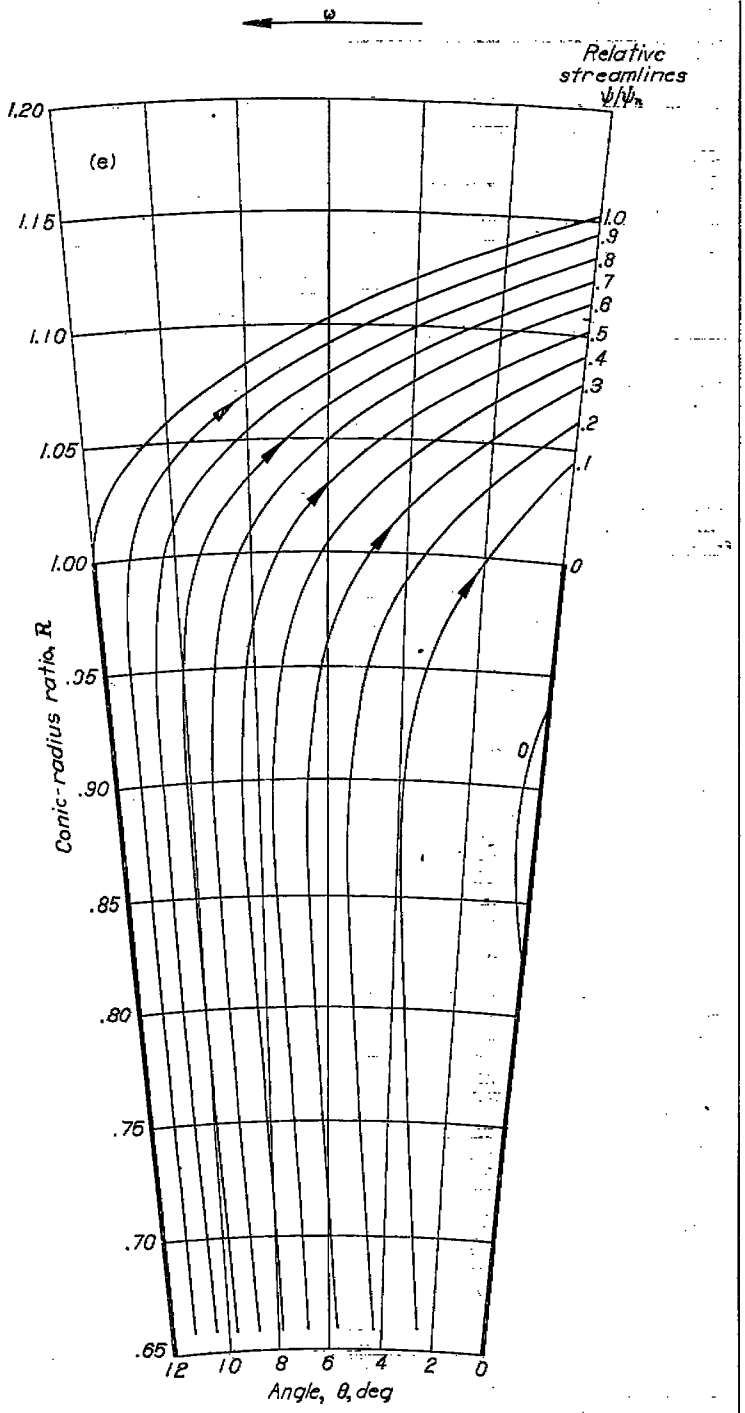


(e) Example 4: varying flow area ($m$,−1.4); other parameters same as standard example.

FIGURE 7.—Continued. Relative streamlines for flow through centrifugal compressor with straight blades. Streamline designation indicates ratio of flow that lies between streamline and positive blade surface (right side of passage) to total flow in passage.

The exponent $m$ determines the change in flow area through the impeller and the diffuser. For $m$ equal to −1.4 (example 4), the flow-area ratio (flow area divided by flow area at impeller tip) at a radius ratio of 0.5 is 1.32 compared to a ratio of 1.0 for the standard example (in which $m$ equals −1.0). The effect of $m$ on the streamline configuration in the flow region investigated is inappreciable (compare figs. 7 (a) and 7 (e)). The reason for this small effect is that the flow areas at the impeller tip are the same (because $\varphi$ is the same) and for reasonable values of $m$ are not much different anywhere in the flow region investigated (which is in the vicinity of the tip, fig. 6). If the area ratio 1.32 had been obtained by maintaining equal flow areas for both impellers at the radius ratio 0.5 within the impellers and decreasing the area at the impeller tip in one case, the streamline configuration would be greatly affected. This effect, however, would not be the result of the change in $m$ but rather of the change in $\varphi$ (which results from the change in $a_T$).

The large effect of compressibility on the streamline configuration (and therefore on the other flow conditions) is shown by a comparison of figures 7 (f) and 7 (g). The large eddy that exists for compressible flow completely disappears for incompressible flow.

**Mach number lines.**—Lines of constant Mach number relative to the impeller are shown for the seven examples in figure 8. It should be noted that the Mach number in the incompressible solution (fig. 8 (g)) is a fictitious quantity that is equal to the fluid velocity $q$ divided by a constant that is equal to the inlet stagnation speed of sound $c_o$ of whatever compressible solution with which the incompressible solution is being compared. This inlet stagnation speed of sound is also contained in the definitions of $\varphi$ and $M_T$, so that for the incompressible solution $q/c_o$, $\varphi$, and $M_T$ vary inversely with the assigned value of $c_o$, but ratios of these parameters are unaffected.

The standard example is given in figure 8 (a). The general characteristics of these plots are similar. The velocities (as indicated by the Mach number lines) along the positive blade surface are low; the velocities along the negative blade surface are high; and the velocities become equal on the positive and negative blade surfaces at the blade tip (as required by the Joukowski condition). The maximum Mach number occurs on the negative blade surface at a radius ratio well within the impeller and the flow decelerates along the blade surface from this point to the blade tip. This deceleration, which for impellers with straight blades and the usual type of area variation with radius ratio becomes rapid near the blade tip, is conducive to boundary-layer separation, which lowers the compressor efficiency.

If the boundary-layer wake in the vaneless diffuser is neglected, the velocities become essentially uniform at a radius ratio of approximately 1.10 for $\Delta\theta$ equal to 12° (figs. 8 (a) to 8 (e)) and at a radius ratio of approximately 1.15 for $\Delta\theta$ equal to 18° (figs. 8 (f) and 8 (g)). These radius ratios and their corresponding angles are equivalent to a value of $\xi$ approximately equal to 0.45. Flow conditions in the vaneless portion of the diffuser immediately following the impeller therefore become essentially uniform at a value of $\xi$ approximately equal to 0.45.

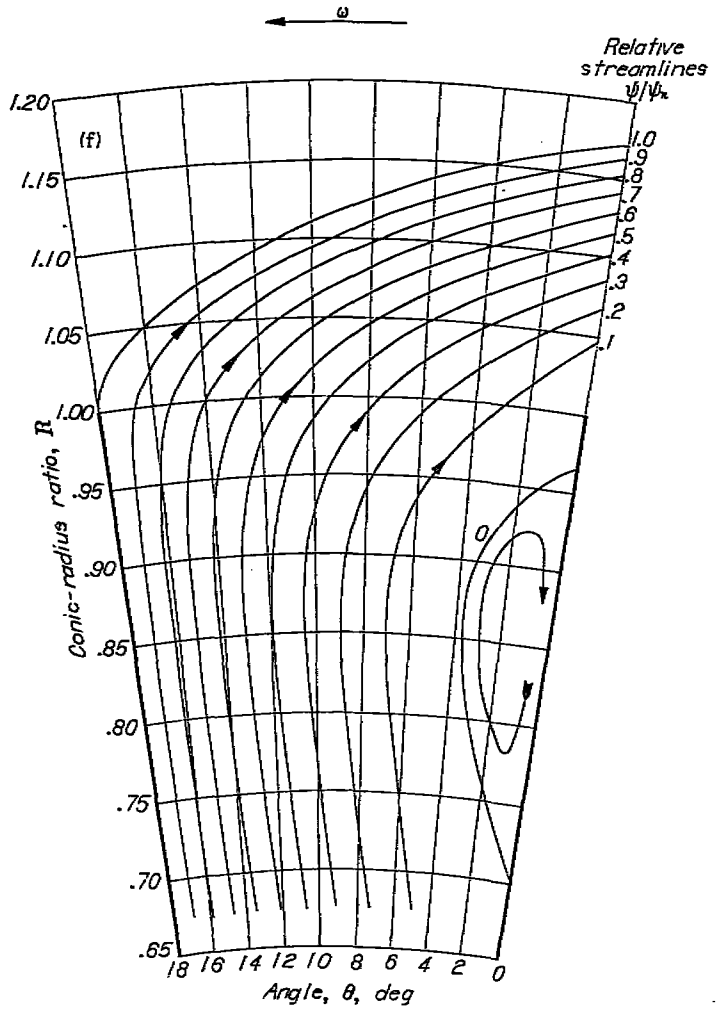


(f) Example 5: angle between blades on conic flow surface $\Delta\theta$, 18°; other parameters same as standard example.

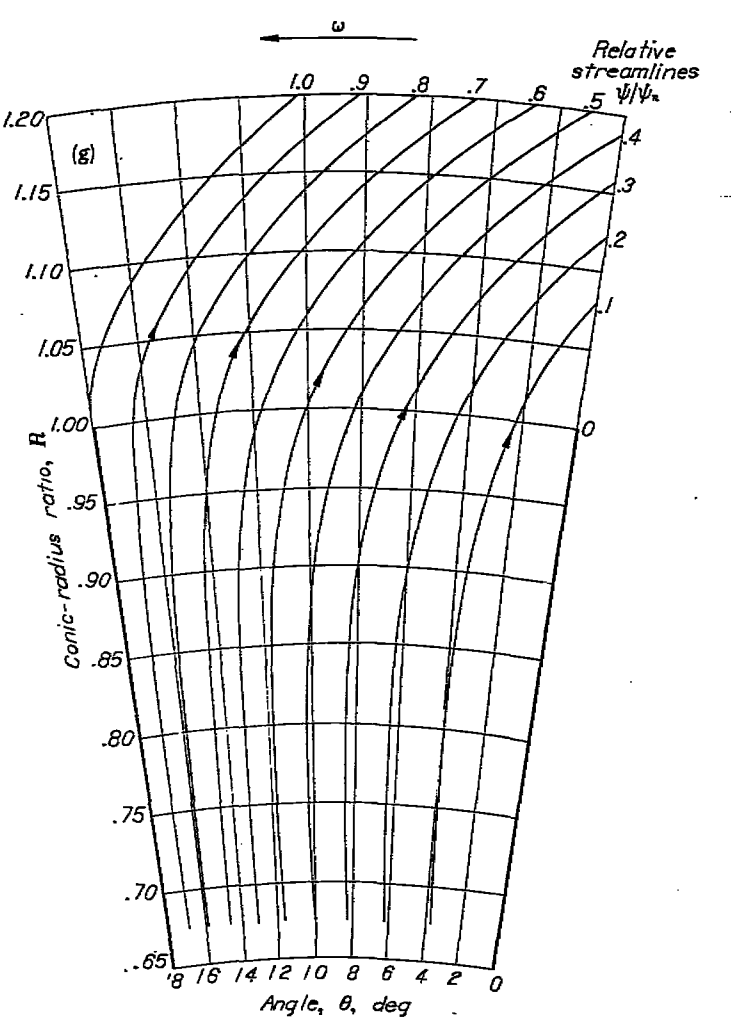


(g) Example 6: incompressible fluid; other parameters same as example 5 (fig. 7(f)). Note that $\varphi$ and $M_T$ are based upon constant $c_a$, which if considered equal to speed of sound at inlet conditions of example 5 enables comparison of compressible (example 5) and incompressible (example 6) solutions for same impeller-tip speed, weight-flow rate, and so forth.

FIGURE 7.—Concluded. Relative streamlines for flow through centrifugal compressor with straight blades. Streamline designation indicates ratio of flow that lies between streamline and positive blade surface (right side of passage) to total flow in passage.

For the compressible-flow examples, the relative Mach number at the impeller tip is low (even for large values of $\varphi$) because of the high density ratios, which result from the high impeller-tip speed. These velocities would be considerably higher if the effective flow area were reduced by boundary-layer separation, which might be expected in practice.

From an inspection of figures 8 (a) to 8 (g), it appears that the maximum Mach number (on the negative blade surface) is increased by increasing the flow coefficient $\varphi$ (figs. 8 (b) and 8 (c)), is apparently not much affected by increasing the impeller-tip Mach number $M_T$ (fig. 8 (d)) or by changing the exponent $m$ (fig. 8 (e)), and is increased by increasing the angle between blades on the conic flow surface $\Delta\theta$ (fig. 8 (f)) or by changing to an incompressible fluid (fig. 8 (g)) (in which the Mach number is a fictitious quantity, as previously indicated).

Slip factor.—The impeller slip factor is defined as the ratio of the average absolute tangential velocity of the fluid at the impeller tip to the tip speed of the impeller. The slip factor has been computed for each of the seven examples by methods given in reference 1. The resulting slip factors are given in the following table:

| Example | Nonstandard parameter | Slip factor |
|---|---|---|
| Standard | | 0.934 |
| 1 | $\varphi$=0.7 | .937 |
| 2 | $\varphi$=0.9 | .938 |
| 3 | $M_T$=2.0 | .935 |
| 4 | $m$=−1.4 | .934 |
| 5 | $\Delta\theta$=18° | .899 |
| 6 | $p/p_a$=1.0[a] | .892 |

[a]Also, $\Delta\theta$=18°.

It appears that the only variable investigated that affects the computed slip factor is the angle between blades on the conic flow surface $\Delta\theta$. In particular, it will be noted that

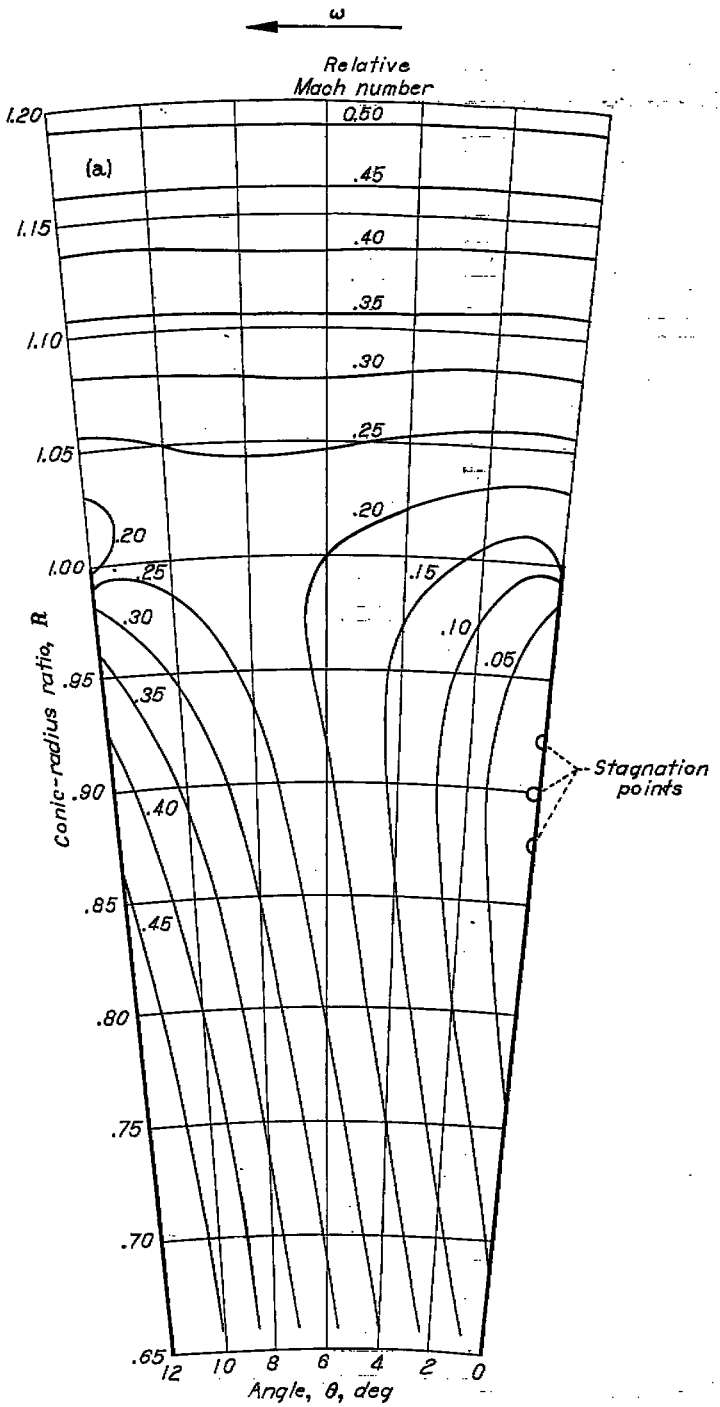


(a) Standard example: flow coefficient $\varphi$, 0.5; impeller-tip Mach number $M_T$, 1.5; constant flow area ($m$,—1.0); angle between blades on conic flow surface $\Delta\beta$, 12°; compressible flow ($\gamma$, 1.4).

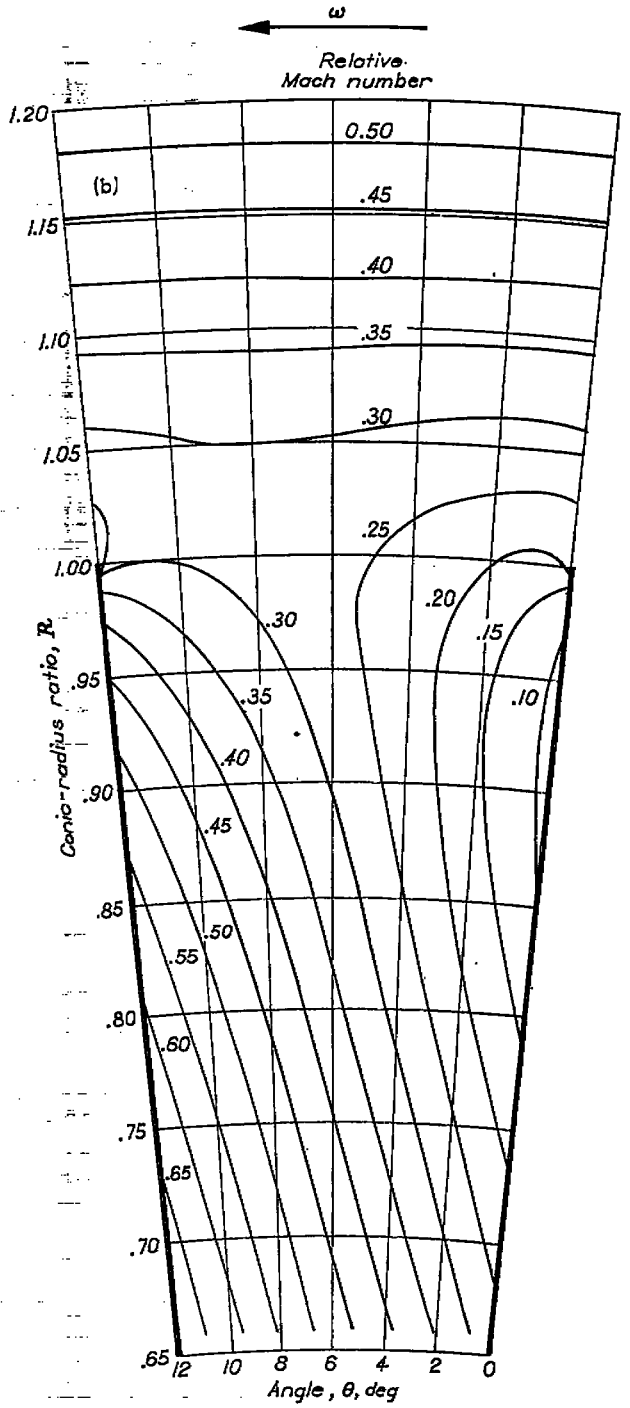


(b) Example 1: flow coefficient $\varphi$, 0.7; other parameters same as standard example.

FIGURE 8.—Lines of constant Mach number relative to impeller.

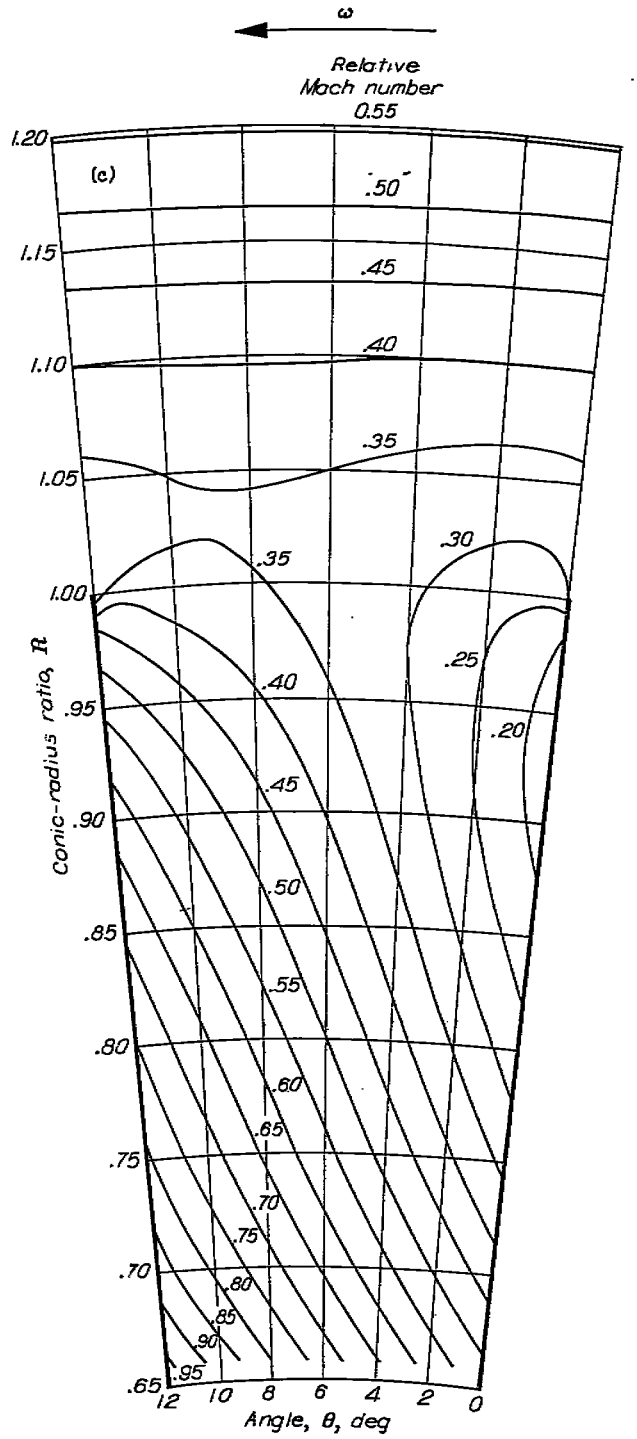


(c) Example 2: flow coefficient $\varphi$, 0.9; other parameters same as standard example.

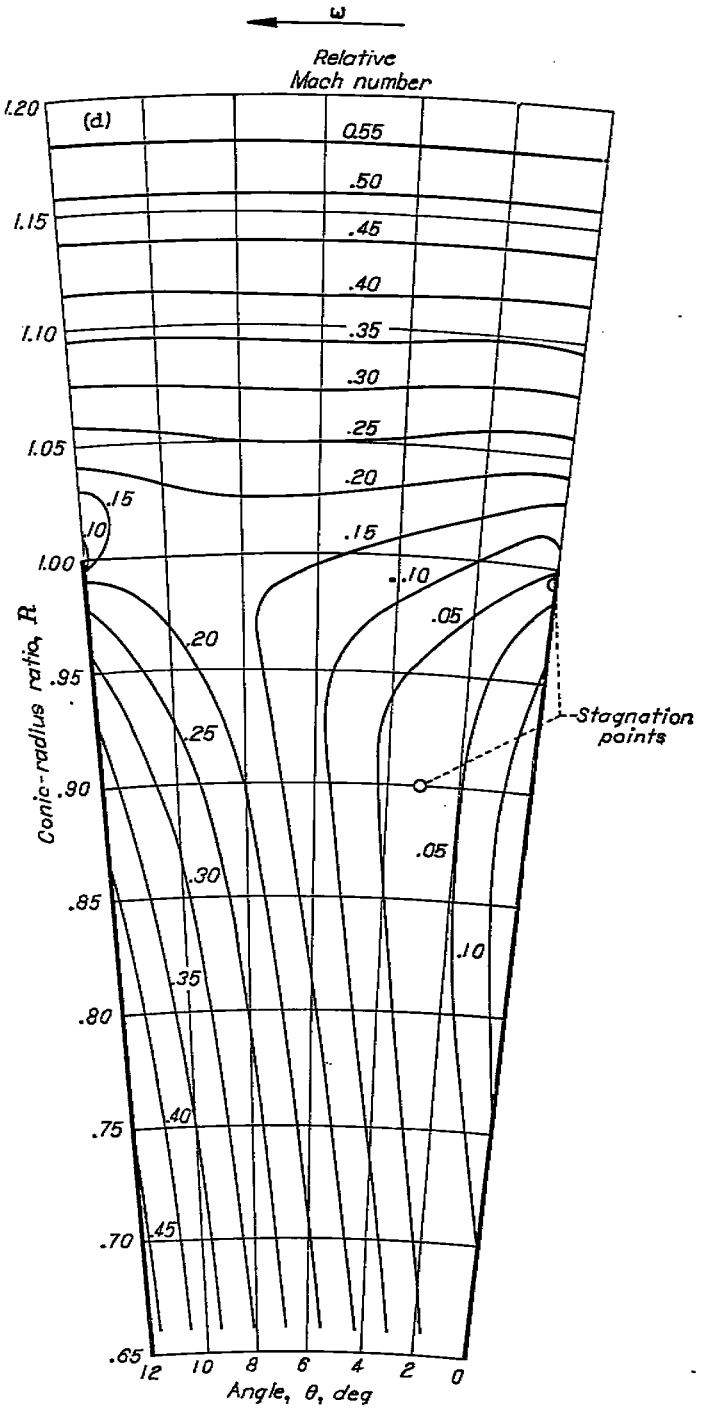


(d) Example 3: impeller-tip Mach number $M_T$, 2.0; other parameters same as standard example.

FIGURE 8.—Continued. Lines of constant Mach number relative to impeller.

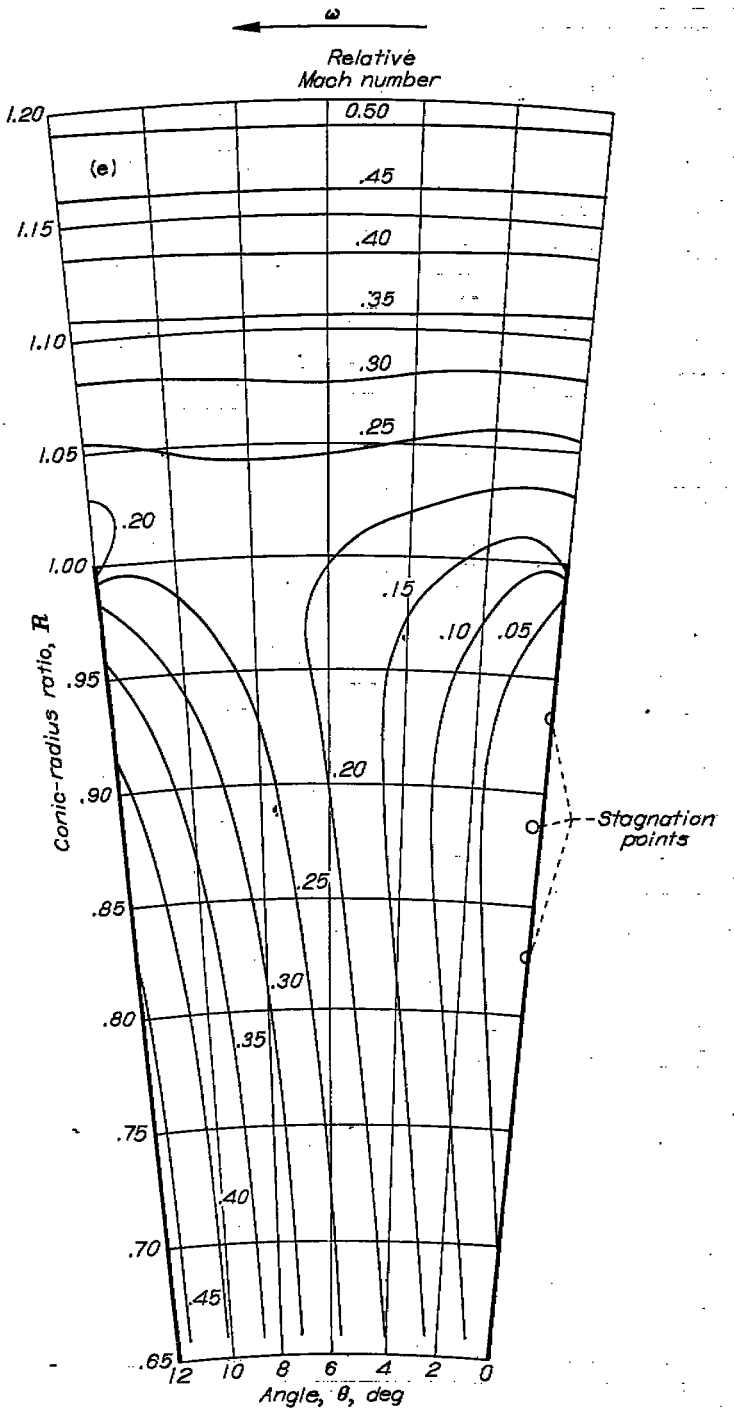


(e) Example 4: varying flow area ($m$, —1.4); other parameters same as standard example.

FIGURE 8.—Continued. Lines of constant Mach number relative to impeller.

the slip factor is approximately the same for compressible and incompressible flow (compare examples 5 and 6), although the streamline configurations for the two examples are very different (compare figs. 7 (f) and 7 (g)).

## CORRELATION OF RESULTS

Correlation equations are presented whereby the flow conditions ($U$, $V$, $\psi/\psi_n$, and so forth) within any impeller with straight blades can be determined (for the flow region investigated herein, see fig. 6) from the flow conditions for the standard solution of this report. These correlation equations are developed in appendix B and the flow conditions for the standard solution are given in tables I to III.

The correlation equations are developed in terms of the transformed coordinates ($\xi$ and $\eta$). The dimensionless conic coordinates $R$ and $\theta$ are related to these transformed coordinates by

$$R=exp(\xi\Delta\theta) \tag{B3}$$

and

$$\theta=\eta\Delta\theta \tag{B4}$$

**Stream-function ratio $\psi/\psi_n$.**—The stream-function ratio $\psi/\psi_n$ varies across the impeller passage from 0 along the positive blade surface of one blade to 1.0 along the negative blade surface of the next blade. At any given point ($\xi$ and $\eta$) within the impeller, the value of the stream-function ratio for any impeller (with straight blades) and for any operating condition can be estimated by the following correlation equation (appendix B):

$$\frac{\psi'}{\psi_n}=\eta+\frac{A}{V_m}\left(\left[V_m\left(\frac{\psi}{\psi_n}-\eta\right)\right]_s+\eta(\eta-1)\left\{\frac{U_s}{2}\left[\Delta\theta-(\Delta\theta)_s\right]+(R-R_s)(M_T\Delta\theta)_s\right\}\right) \tag{B16}$$

where the prime indicates the estimated value of flow condition (stream-function ratio in this case) at a given point ($\xi$,$\eta$) and the subscript $s$ indicates the standard value of flow condition at the same point. Also,

$$A=\frac{M_T\Delta\theta}{(M_T\Delta\theta)_s} \tag{B2}$$

$$V_m=\frac{\varphi}{\frac{\rho_m}{\rho_o}RH} \tag{B9}$$

and, if the absolute whirl ahead of the impeller is zero,

$$\frac{\rho_m}{\rho_o}=\left\{1+\frac{\gamma-1}{2}\left[(RM_T)^2-\left(\frac{\varphi}{\frac{\rho_m}{\rho_o}RH}\right)^2\right]\right\}^{\frac{1}{\gamma-1}} \tag{B10}$$

where the subscript $m$ indicates the mean value at a given radius ratio $R$ (that is, at a given value of $\xi$, which is related to $R$ by equation (10a)).

The estimated values of the stream-function ratio $\psi'/\psi_n$ obtained from the correlation equation (B16) are compared in figure 9 with the relaxation values of $\psi/\psi_n$ obtained for the numerical examples of this report. Values are plotted for every other grid point across the passage at values of $\xi$ indicated by the symbols. Perfect correlation corresponds to

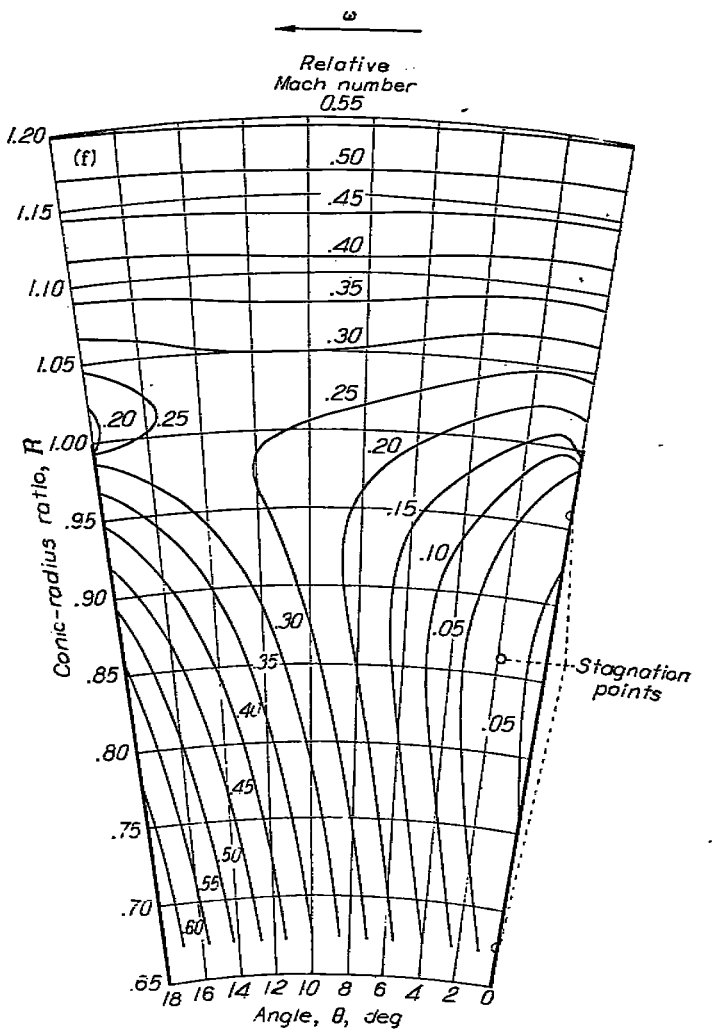


(f) Example 5: angle between blades on conic flow surface $\Delta\theta$, 18°; other parameters same as standard example.

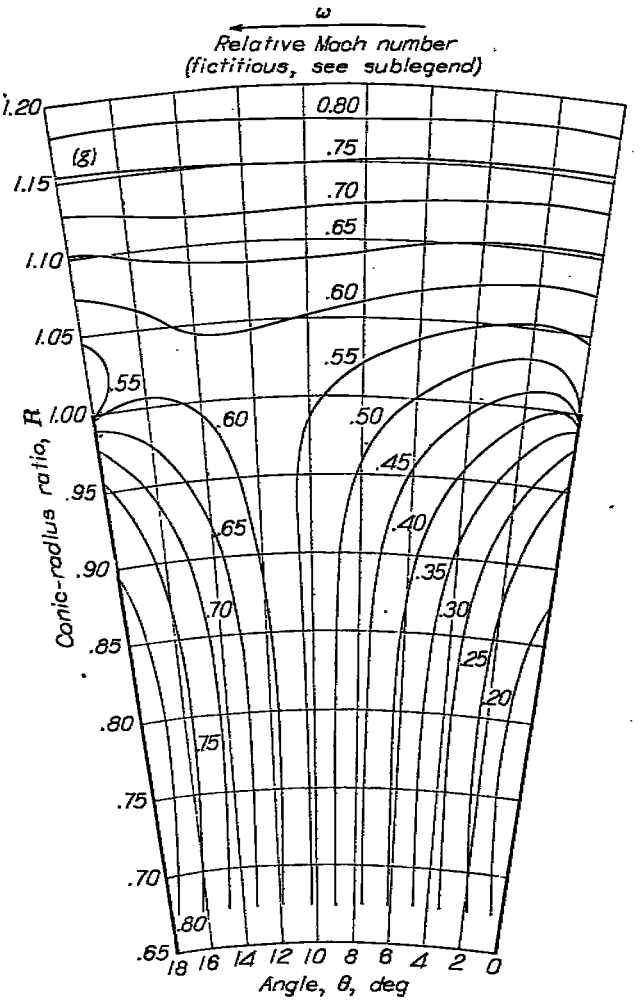


(g) Example 6: incompressible fluid; other parameters same as example 5 (fig. 8 (f)). Note that $\varphi$ and $M_T$ are based upon constant $c_a$, which if considered equal to speed of sound at inlet conditions of example 5 enables comparison of compressible (example 5) and incompressible (example 6) solutions for same impeller-tip speed, weight-flow rate, and so forth. For incompressible fluids the relative Mach number is fictitious and is equal to relative velocity $q$ divided by constant $c_a$.

FIGURE 8.—Concluded. Lines of constant Mach number relative to impeller.

the 45° line on this plot. The error is, with very few exceptions, less than 0.01, where the error is defined as

$$\text{Error}=\left(\frac{\psi'}{\psi_n}-\frac{\psi}{\psi_n}\right)$$

The negative values of $\psi/\psi_n$ shown on the correlation plot correspond to eddies, which were shown in the previous section to form on the positive blade surface at low flow rates and at high tip speeds. The stream-function ratio is always zero at the positive blade surface and always 1.0 at the negative blade surface.

**Radial-velocity ratio** $V$.—The radial-velocity ratio can be estimated by the following correlation equation (appendix B):

$$V'=V_m+A(V-V_m)_s+$$
$$A(2\eta-1)\left\{\frac{U_s}{2}\left[\Delta\theta-(\Delta\theta)_s\right]+(R-R_s)(M_T\Delta\theta)_s\right\} \quad \text{(B13)}$$

The estimated values of the radial-velocity ratio $V'$ obtained from equation (B13) are compared in figure 10 with the values of $V$ obtained from the relaxation solutions of this report. Values are plotted for every other grid point across the passage at the values of $\xi$ indicated by the symbols. Perfect correlation corresponds to the 45° line on this plot. The error is less than 0.01 where the error is defined as

$$\text{Error}=(V'-V)$$

The negative values of $V$ shown in the correlation plot correspond to the eddies that form on the positive blade surface at low flow rates and at high tip speeds.

**Tangential-velocity ratio** $U$.—The relative tangential-velocity ratio can be estimated by the following correlation equation (appendix B):

$$U'=AU_s \quad \text{(B1)}$$

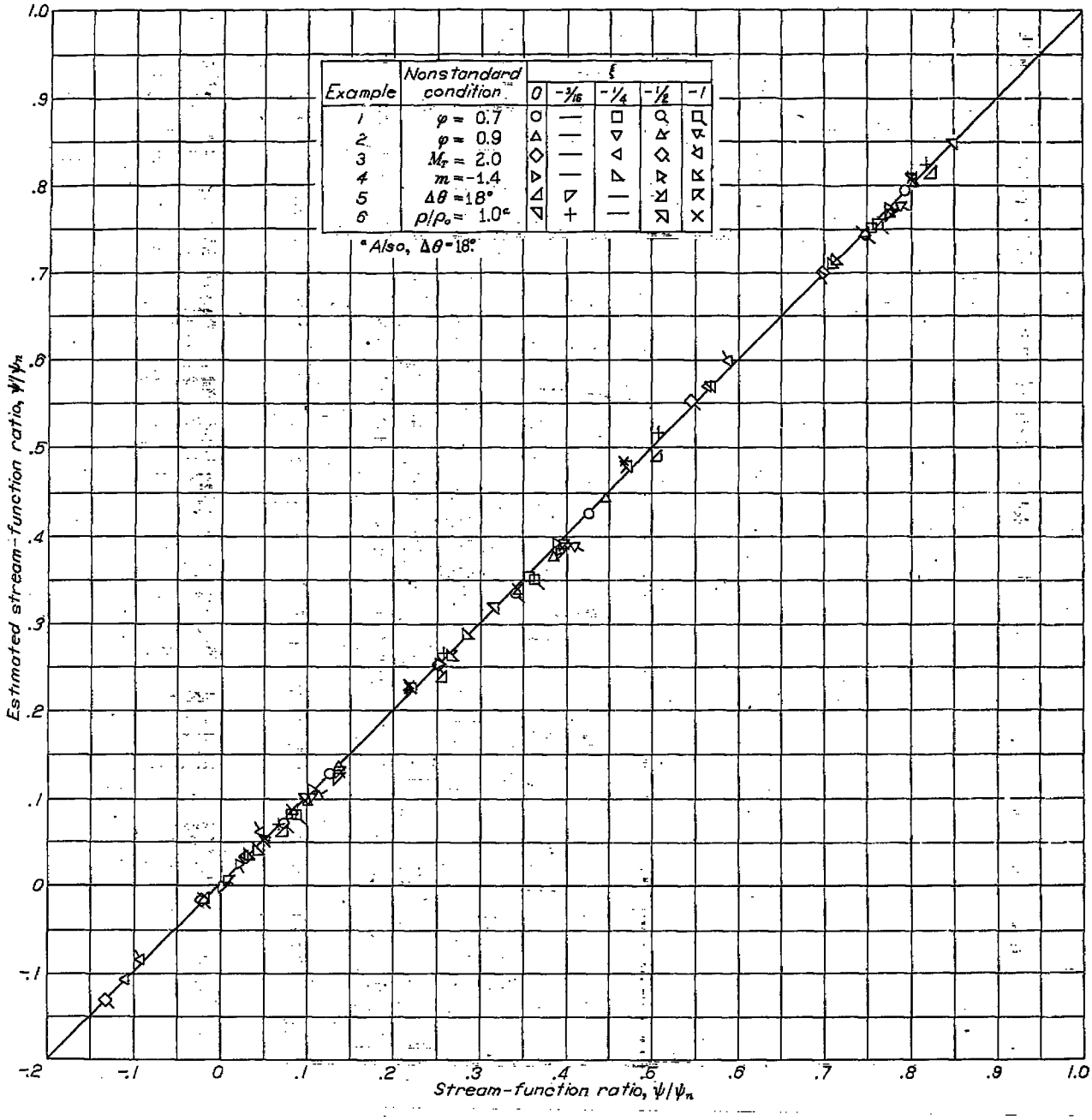


FIGURE 9.—Comparison between exact (relaxation solution) and estimated (correlation equation (B16)) values of stream-function ratio for various values of $R$ (function of $\xi$ and $\Delta\theta$) and $\theta$.

The estimated values of the relative tangential-velocity ratio $U'$ obtained from equation (B1) are compared in figure 11 with the values of $U$ obtained from the relaxation solutions of this report. Values are plotted for every grid point across the first half of the passage for the values of $\xi$ indicated by the symbols. Perfect correlation corresponds to the 45° line on this plot. Except for the incompressible solution (example 6), the error is less than 0.01 where the error is defined as

$$\text{Error} = (U' - U)$$

The relative tangential-velocity ratio is always zero along the blade surfaces.

**Other flow conditions.**—Other flow conditions within the impeller can be determined from the values of $U$ and $V$ obtained by the correlation equations (B1) and (B13). The relative velocity ratio $Q$ is given by

$$Q^2 = U^2 + V^2 \tag{13}$$

From the steady-flow energy equation, the temperature ratio is given by (equation (10), reference 1)

$$\frac{T}{T_0} = 1 + \frac{\gamma - 1}{2}\left[(R M_T)^2 - Q^2\right]$$

where $T$ is the absolute static temperature of the gas and where the absolute whirl ahead of the impeller is assumed to be zero.

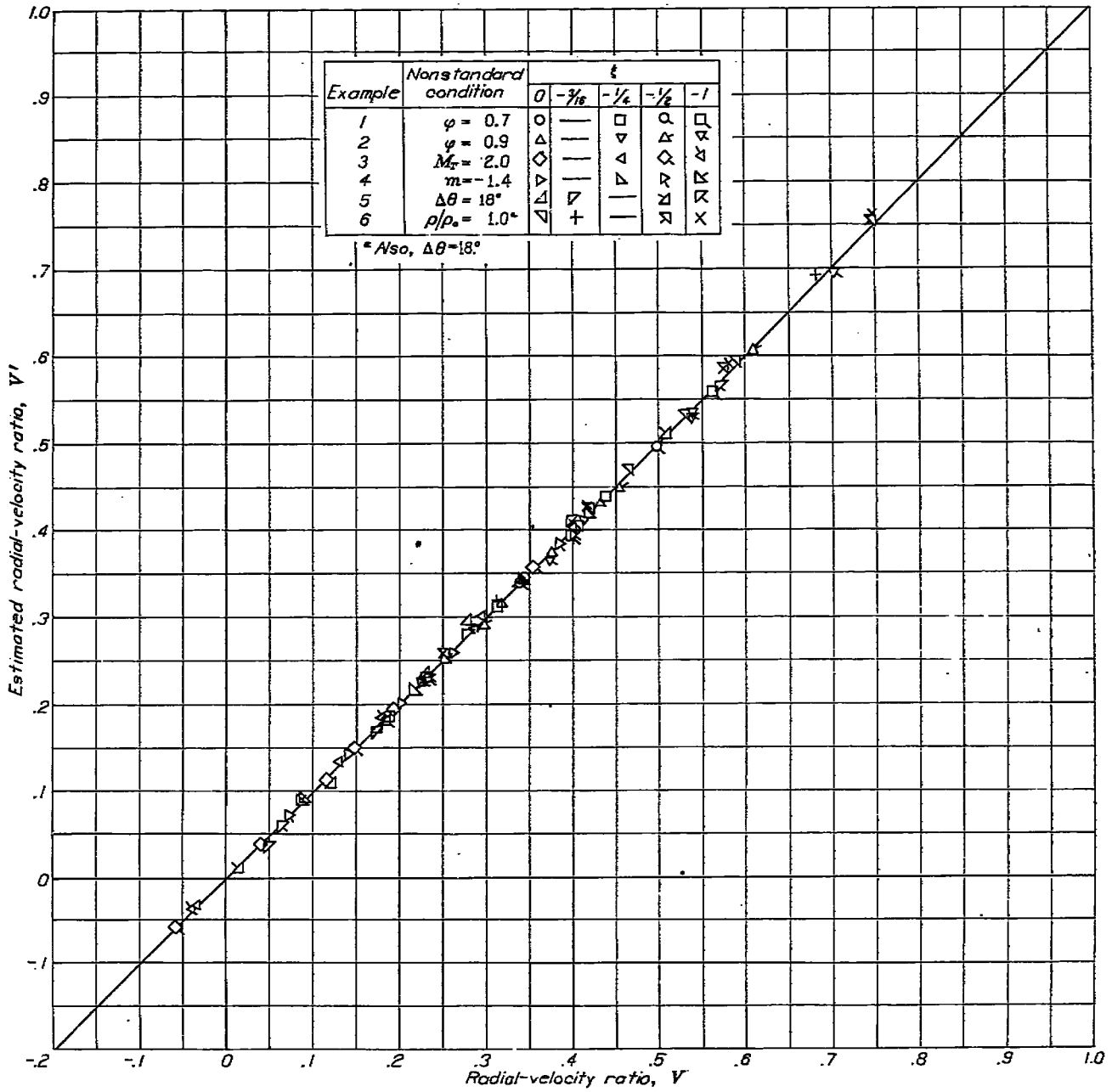


FIGURE 10.—Comparison between exact (relaxation solution) and estimated (correlation equation (B13)) values of radial-velocity ratio for various values of $R$ (function of $\xi$ and $\Delta\theta$) and $\theta$.

The density ratio $\rho/\rho_o$ and the pressure ratio $p/p_o$ are obtained from the temperature ratio by

$$\frac{\rho}{\rho_o}=\left(\frac{T}{T_o}\right)^{\frac{1}{\gamma-1}}=\left\{1+\frac{\gamma-1}{2}\left[(RM_T)^2-Q^2\right]\right\}^{\frac{1}{\gamma-1}} \qquad (12)$$

and

$$\frac{p}{p_o}=\left(\frac{T}{T_o}\right)^{\frac{\gamma}{\gamma-1}}=\left\{1+\frac{\gamma-1}{2}\left[(RM_T)^2-Q^2\right]\right\}^{\frac{\gamma}{\gamma-1}}$$

The local relative Mach number is related to $Q$ and the temperature ratio by

$$M=Q\sqrt{\frac{T_o}{T}}$$

**Correlation of velocities along blade surfaces.**—Of special interest, because of boundary-layer considerations, are the velocity distributions along the positive and negative surfaces of the impeller blades, $Q_p$ and $Q_n$. Estimated values of $Q_n$ obtained from the correlation equations are given by the curves in figure 12 for each of the numerical examples in this report. The values of $Q_n$ obtained by the relaxation solution are shown by the plotted points. The agreement is seen to be excellent in all cases.

Estimated values of $Q_p$ obtained from the correlation equations are given by the curves in figure 13 for each of the numerical examples in this report. The values of $Q_p$ obtained by the relaxation solution are shown by the plotted points. Again the agreement is excellent.

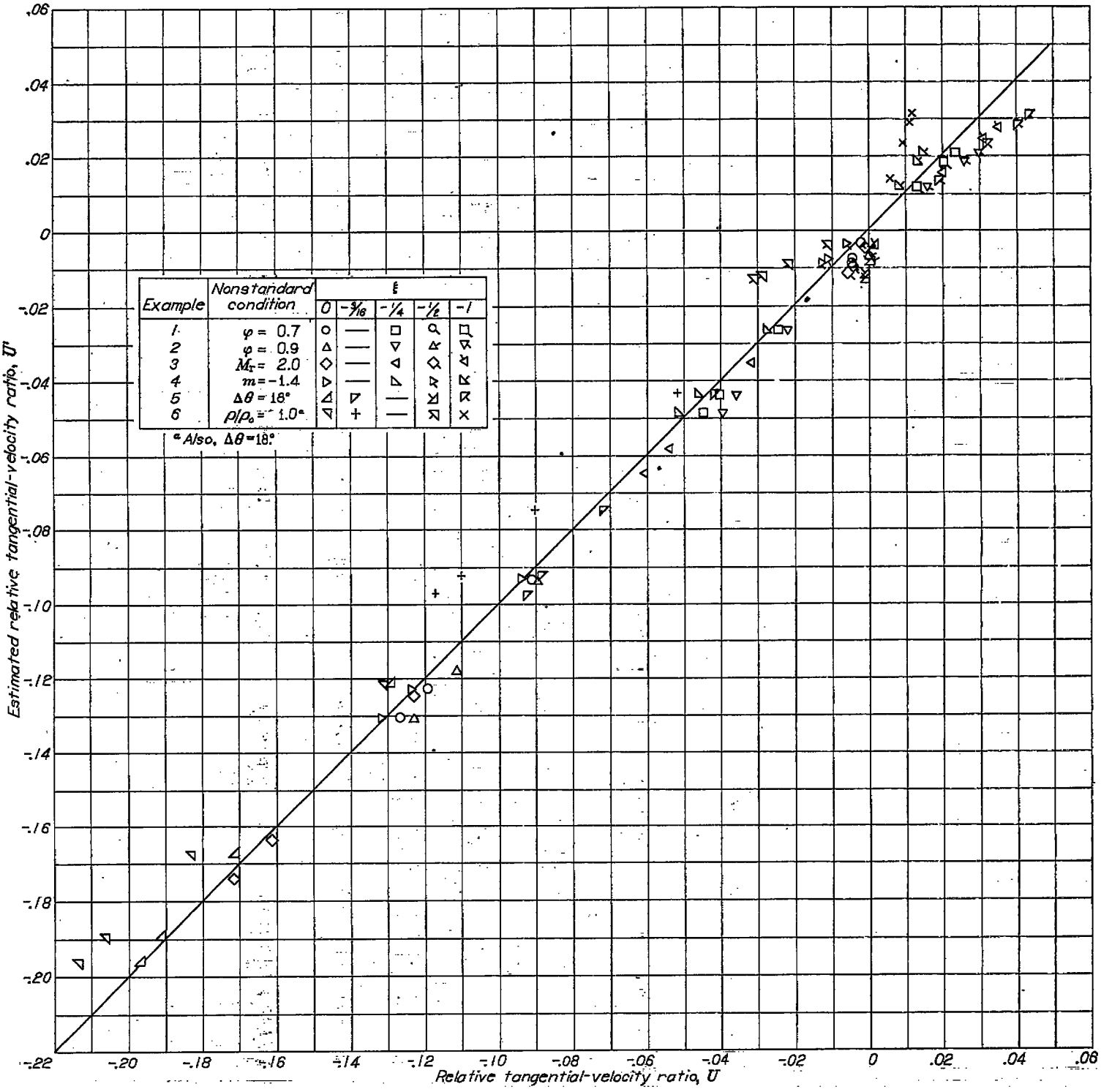


FIGURE 11.—Comparison between exact (relaxation solution) and estimated (correlation equation (B1)) values of relative tangential-velocity ratio for various values of $R$ (function of $\xi$ and $\Delta\theta$) and $\theta$.

**Slip factor.**—The impeller slip factor $\mu$ is defined as the ratio of the absolute tangential velocity of the fluid at the impeller tip to the tip speed of the impeller. The following correlation equation is developed in appendix C for the slip factor of impellers with straight blades:

$$\mu'=1-(1-\mu_s)\frac{\Delta\theta}{(\Delta\theta)_s} \qquad \text{(C2)}$$

For the standard solution, $(\Delta\theta)_s$ is 0.2095 radian and $\mu_s$ is 0.934 so that the slip-factor equation becomes

$$\mu'=1-0.315\Delta\theta \qquad (17)$$

This equation is plotted in figure 14 together with Stodola's equation, which for straight blades is given by

$$\mu=1-0.500\Delta\theta \qquad (18)$$

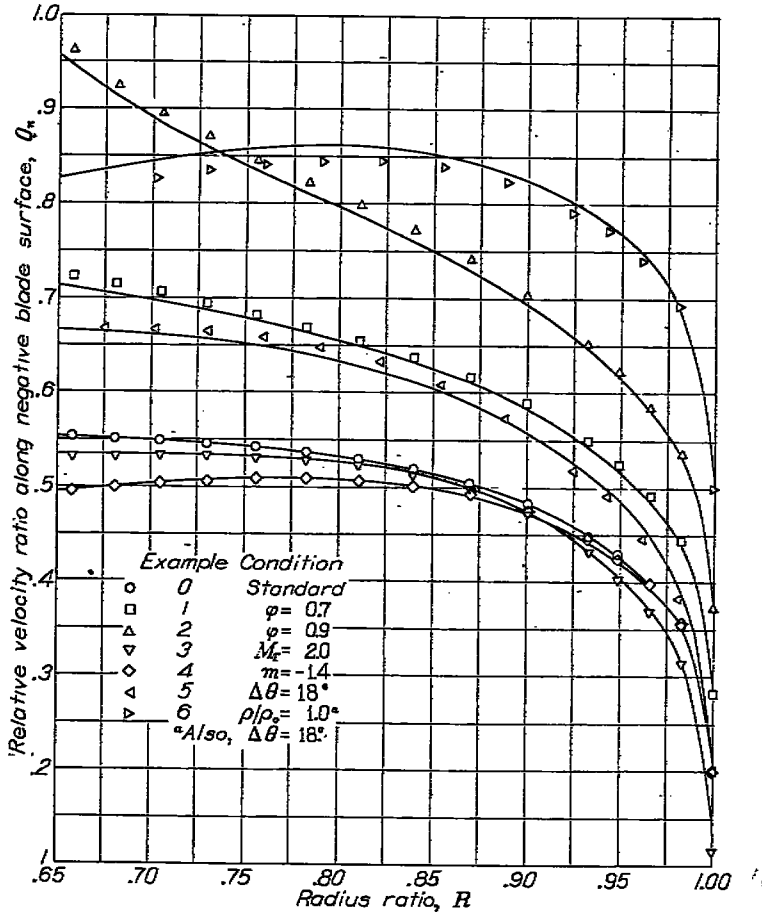


FIGURE 12.—Comparison between exact (relaxation solution) and estimated (correlation equation (B13)) values of relative velocity ratio along negative blade surface. Solid lines obtained from correlation equation; plotted points obtained from relaxation solution.

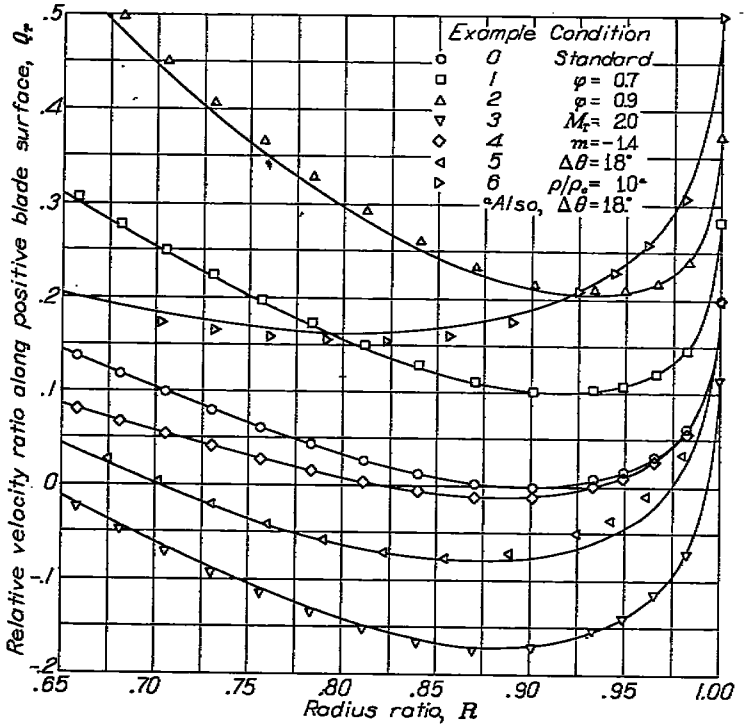


FIGURE 13.—Comparison between exact (relaxation solution) and estimated (correlation equation (B13)) values of relative velocity ratio along positive blade surface. Solid lines obtained from correlation equation; plotted points obtained from relaxation solution.

The slip factors obtained for the numerical examples of this report are plotted as points in figure 14. These points indicate that the slip factor is independent of the flow rate, impeller-tip speed, and variation in passage-height ratio with radius and depends only on the angle between blades on the conic flow surface $\Delta\theta$. This conclusion is in agreement with Stodola's equation although the magnitude of the slip factor given by Stodola is lower.

## APPLICATION OF CORRELATION EQUATIONS

The correlation equations presented in the previous section are important because they provide rapid solutions (in the regions investigated herein, fig. 6) to the differential equation, which determines the flow conditions ($U$, $V$, $p/p_o$, and so forth) in any impeller (with straight blades) for all operating conditions. An important application of the correlation equations is the determination of velocities along the flow surfaces because these velocities are significant in the study of the boundary layer. As examples of the information provided by the correlation equations for such a study, the velocity ratios along the blade surfaces have been computed over a wide range of impeller-tip Mach number $M_T$, flow coefficient $\varphi$, and angle between blades on the conic flow surface $\Delta\theta$. These computations are presented in figures 15 to 17.

**Impeller-tip Mach number $M_T$.**—The effect of $M_T$ on the velocity ratios along the positive and negative blade surfaces is shown in figure 15. In this figure all design and operating conditions (other than $M_T$) were maintained constant at the standard values.

For $M_T$ equal to zero, the velocities are equal on both surfaces of the blade. For all other values of $M_T$, the relative velocities are higher on the negative blade surface than on the positive blade surface and as the impeller-tip speed increases the difference in velocities along the two surfaces increases. Except near the tip, this increase in velocity difference results primarily from a decrease in velocity along the positive blade surface and for high values of $M_T$ this velocity becomes negative, which indicates the presence of an eddy. The small effect of $M_T$ on $Q_n$ results from a combination of effects. At higher values of $M_T$, the difference between $Q_n$ and the mean radial-velocity ratio $V_m$ increases, but $V_m$ itself decreases because of the increased density; the net result is only a small change in $Q_n$ with

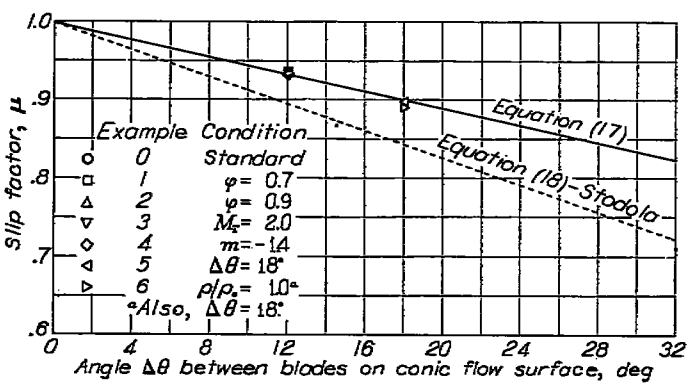


FIGURE 14.—Comparison among slip factors obtained from relaxation solutions, correlation equation (17), and Stodola's equation (18).

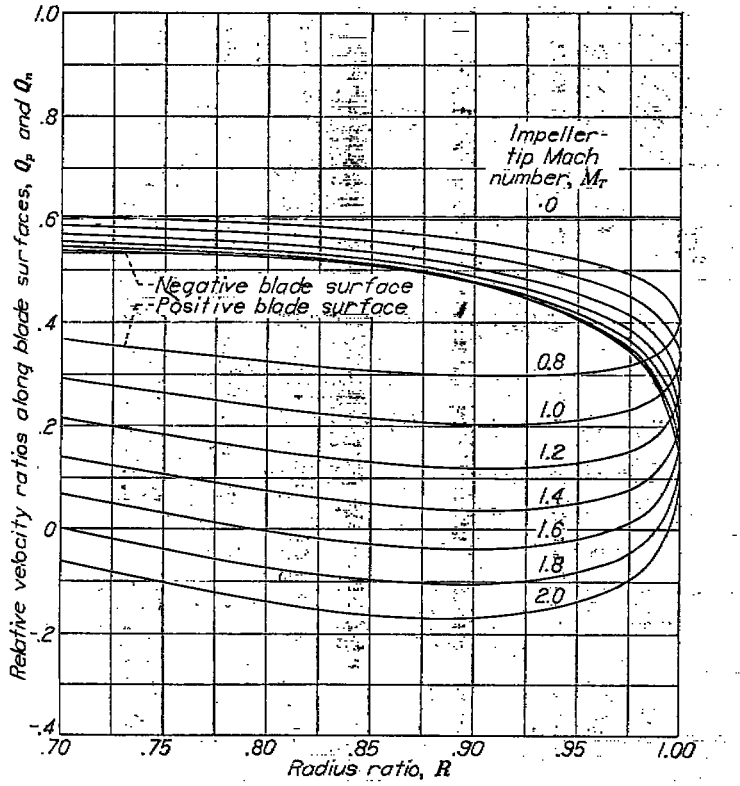


FIGURE 15.—Effect of impeller-tip Mach number on relative velocity ratio along positive and negative blade surfaces. Correlation equation (B13); flow coefficient $\varphi$, 0.5; constant flow area ($m$,—1.0); angle between blades on conic flow surface $\Delta\theta$, 12°; compressible flow ($\gamma$, 1.4).

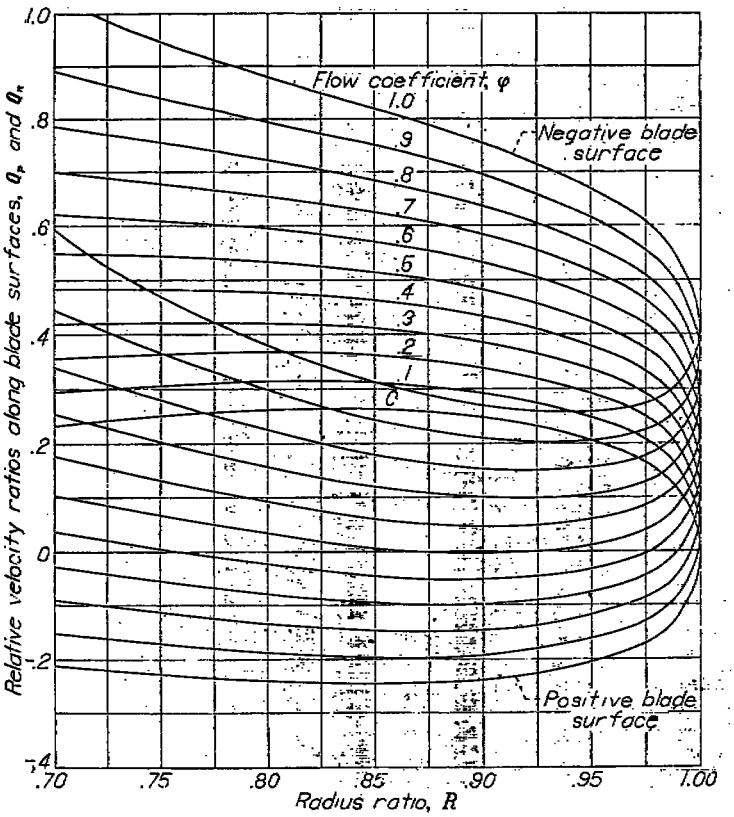


FIGURE 16.—Effect of flow coefficient on relative velocity ratio along positive and negative blade surfaces. Correlation equation (B13); impeller-tip Mach number $M_T$, 1.5; constant flow area ($m$,—1.0); angle between blades on conic flow surface $\Delta\theta$, 12°; compressible flow ($\gamma$, 1.4).

changes in $M_T$. At the blade tip, the velocity becomes equal on both surfaces and this velocity decreases with increasing $M_T$ because of the higher gas density.

**Flow coefficient $\varphi$.**—The effect of flow coefficient $\varphi$ on the velocity ratios along the positive and negative blade surfaces is shown in figure 16. In this figure, all design and operating conditions (other than the flow coefficient) were maintained constant at the standard values.

At each radius ratio, the difference between $Q_n$ and $Q_p$ is independent of $\varphi$ (that is, remains constant). The mean radial-velocity ratio $V_m$, however, decreases with decreasing flow coefficient and for low flow coefficients $Q_p$ becomes negative, which indicates the presence of an eddy. At the blade tip, the velocity becomes equal on both surfaces and this velocity increases with increasing flow coefficient because of the increased mean radial velocity $V_m$.

For $\varphi$ equal to zero, the velocities are equal on both surfaces of the blade (but opposite in sign). As a result the pressures on both blade surfaces are equal and no work is done by the impeller. The entire flow within the passage is an eddy.

**Angle between blades on conic flow surface $\Delta\theta$.**—The effect of $\Delta\theta$ on the velocity ratios along the positive and negative blade surfaces is shown in figure 17. In this figure all design and operating conditions other than $\Delta\theta$ were maintained constant at the standard values. Increased values of $\Delta\theta$ indicate fewer blades.

The correlation equation (B13) used to obtain the curves plotted in figure 17 is developed in terms of the transformed

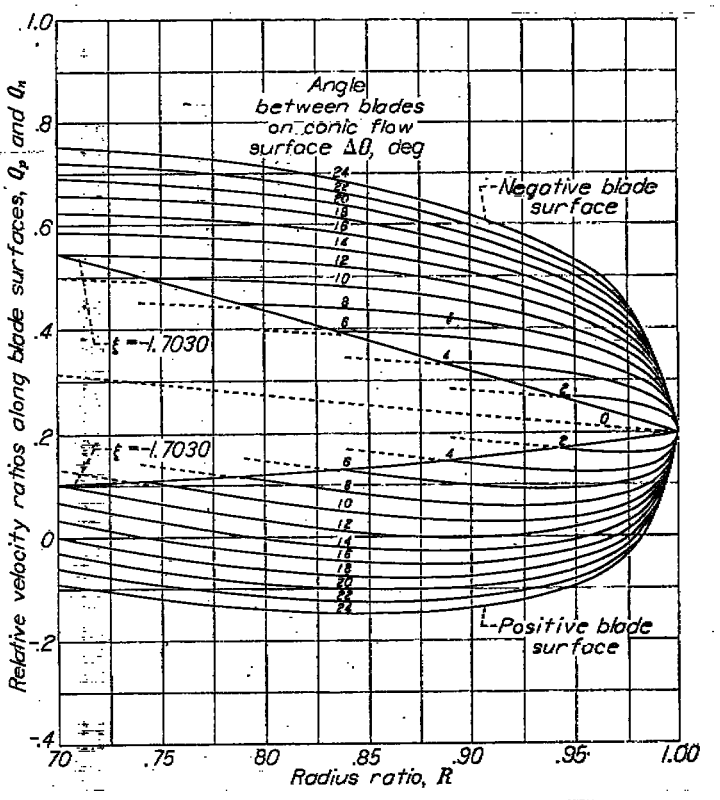


FIGURE 17.—Effect of angle between blades on conic flow surface $\Delta\theta$ on relative velocity ratio along positive and negative blade surfaces. Correlation equation (B13); dashed lines obtained from simplified analysis (equation (19)); flow coefficient $\varphi$, 0.5; impeller-tip Mach number $M_T$, 1.5; constant flow area ($m$,—1.0); compressible flow ($\gamma$, 1.4).

coordinate $\xi$, which is related to the radius ratio $R$ by an expression (equation (B3)) that includes the angle between blades on the conic flow surface $\Delta\theta$. The minimum value of $\xi$ for which standard values of $U$, $V$, and so forth are given in tables I to III is $-1.7030$, which for values of $\Delta\theta$ less than standard ($\Delta\theta=12°$) corresponds to values of $R$ greater than 0.7, as indicated by equation (B3) and shown in figure 17. For values of $R$ less than those resulting from $\xi$ equal to $-1.7030$, however, the simplified analysis presented in reference 1 for impellers with straight blades may be used to extrapolate the curves to all lesser values of $R$. In terms of the mean velocity ratio $V_m$ (equation (B9)), the simplified equation for the velocity ratio becomes (Note that the simplified analysis of reference 1 assumes $U=0$.)

$$Q=V=V_m+RM_T\Delta\theta\left[2\left(\frac{\theta}{\Delta\theta}\right)-1\right] \tag{19}$$

where $V$ equals $V_m$ midway between blades (that is, when $\theta=\Delta\theta/2$). Equation (19) has been used to extrapolate the curves for values of $\Delta\theta$ less than 12° in figure 17 (dashed lines). For values of $\xi$ less than $-1.7030$, the simplified analysis given in reference 1 can be used to determine the flow conditions within the impeller passage for any design and operating condition. For values of $\xi$ greater than $-1.7030$, the methods of this report must be used to determine $V$, $p/p_o$, and so forth.

For $\Delta\theta$ equal to zero, the velocities are the same on both surfaces of the blade and are equal to the mean velocity $V_m$ (dashed line). This mean velocity is the same for all values of $\Delta\theta$, but the difference between $V_m$ and $Q_p$ increases with increasing values of $\Delta\theta$ so that, for large values of $\Delta\theta$, $Q_p$ becomes negative, which indicates the presence of an eddy.

## SUMMARY OF RESULTS AND CONCLUSIONS

Six numerical examples are presented for steady, two-dimensional, compressible, nonviscous flow in centrifugal compressors with thin straight blades, the center lines of which generate the surface of a right circular cone when rotated about the axis of the compressor. A seventh example is presented for incompressible flow. The solutions were obtained in a region of the compressors (including the impeller tip) that was considered to be unaffected by the inlet configuration of the impeller and by the diffuser vanes. (That is, the impeller inlet and the diffuser vanes, if any, must be far enough removed from the region investigated not to affect the flow appreciably in that region.) The effects of variations in the following parameters were investigated: (1) flow coefficient (flow rate), (2) impeller-tip Mach number, (3) exponent for the variation of passage-height ratio with radius ratio, and (4) the angle between blades on the conic flow surface. Each solution applies to radial- and mixed-flow compressors (and turbines with the rotation and flow direction reversed) with various cone angles but with the same angle between blades on the conic flow surface. The numerical results are presented in plots of the streamlines and constant Mach number lines.

Correlation equations are developed whereby flow conditions (streamlines, velocities, pressures, impeller slip factor, and so forth) within any impeller with straight blades can be determined (for flow region investigated) from the flow conditions of the standard solution presented. As examples of the information provided by the correlation equations, the velocities along the blade surfaces have been computed (and plotted) over a wide range of impeller-tip Mach number, flow coefficient, and angle between blades on the conic flow surface.

The principal conclusions resulting from the work presented herein are:

1. The exponent $m$, which was used in this analysis to specify the variation in passage-height ratio with radius ratio, has only a small effect (for practical values of $m$) on the area variation in the flow region investigated and therefore has only a small effect on the flow in this region.

2. An eddy forms on the positive blade surface at high impeller-tip Mach numbers, low flow coefficients, and large angles between blades on the conic flow surface. At an impeller-tip Mach number of 2.0 (and the standard values of flow coefficient and angle between blades on the conic flow surface), the eddy occupies more than 50 percent of the flow area at a radius ratio of 0.90.

3. Compressibility has a large effect on the streamline configuration within the compressor (and therefore on the other flow conditions). For example, the large eddy that exists in the compressible-flow example (with the same parameters as the incompressible example) completely disappears in the incompressible example.

4. The maximum relative Mach number occurs on the negative blade surface at a radius ratio well within the impeller, and the flow decelerates along the surface of the blade from this point to the blade tip. This deceleration, which for impellers with straight blades and with the usual type of area variation with radius ratio becomes rapid near the blade tip, is conducive to boundary-layer separation.

5. If the boundary-layer wake in the vaneless diffuser is neglected, the flow conditions in the vaneless diffuser following the impeller become essentially uniform at a value of $\xi$ approximately equal to 0.45.

6. For the high impeller-tip Mach numbers investigated (and if boundary-layer effects are neglected), the relative velocities at the impeller tip are low because the high impeller-tip Mach numbers result in high fluid densities.

7. The maximum relative Mach number (on the negative blade surface) is increased by increasing the flow coefficient or the angle between blades on the conic flow surface (that is, the number of blades), but it is little affected by the impeller-tip Mach number.

8. The impeller slip factor is independent of the impeller-tip Mach number, compressor flow coefficient, variation in passage-height ratio with radius ratio, and compressibility of the fluid. The slip factor is a function only of the angle between blades on the conic flow surface.

9. The difference between velocities on the positive and negative blade surfaces increases with increasing tip Mach number and angle between blades on the conic flow surface but is independent of the flow coefficient.

LEWIS FLIGHT PROPULSION LABORATORY,
NATIONAL ADVISORY COMMITTEE FOR AERONAUTICS,
CLEVELAND, OHIO, *June 21, 1949.*

9766-18 51 -12

# APPENDIX A

## SYMBOLS

The following symbols are used in this report:

| | |
|---|---|
| $A$ | ratio (equation (B2)) |
| $a$ | annular flow area (normal to conic flow surface) |
| $B$ | number of passages (or blades) |
| $b$ | grid spacing (fig. 3) |
| $c$ | local speed of sound |
| $exp$ | exponential, $[exp\ (x)=e^x]$ |
| $H$ | passage-height ratio, $h/h_T$ |
| $h$ | passage height (normal to conic flow surface) |
| $M$ | relative Mach number |
| $M_T$ | impeller-tip Mach number (equation (9)) |
| $m$ | passage-height exponent (equation (11)) |
| $p$ | absolute static pressure |
| $Q$ | relative velocity ratio, $q/c_o$ |
| $q$ | velocity of fluid relative to blades, $u^2+v^2$ |
| $R$ | conic-radius ratio (coordinate of conic flow surface), $r/r_T$ |
| R | residual |
| $r$ | conic radius (distance along conic element from apex of cone) (fig. 1) |
| $T$ | absolute static (stream) temperature |
| $U$ | relative tangential-velocity ratio, $u/c_o$ |
| $u$ | tangential component of $q$ (in positive direction of $\theta$) (fig. 2) |
| $V$ | radial-velocity ratio, $v/c_o$ |
| $v$ | radial component of $q$ (along conic element) (fig. 2) |
| $W$ | total compressor flow rate |
| $\alpha$ | cone angle (fig. 1) |
| $\gamma$ | ratio of specific heats |
| $\eta$ | transformed coordinate (equation (10b)) |
| $\theta$ | angle (coordinate of conic flow surface, positive in counterclockwise direction), radians unless otherwise specified |
| $\Delta\theta$ | angle between blades on conic flow surface (equation (6), (fig. 6)), radians unless otherwise specified |
| $\mu$ | impeller slip factor |
| $\xi$ | transformed coordinate (equation (10a)) |
| $\rho$ | weight density of fluid |
| $\varphi$ | compressor flow coefficient (equation (7)) |
| $\psi$ | dimensionless compressible stream function (equations (4a) and (4b)) |
| $\omega$ | impeller angular velocity (in positive direction of $\theta$) |

Subscripts:

| | |
|---|---|
| $m$ | mean value at given radius ratio |
| $n$ | negative blade surface (blade surface in negative direction of $\theta$) |
| $o$ | absolute stagnation condition in region of uniform flow upstream of impeller |
| $p$ | positive blade surface (blade surface in positive direction of $\theta$) |
| $s$ | standard solution |
| $T$ | impeller tip |
| 1, 2, 3, and 4 | grid points adjacent to point being considered (fig. 3) |

Superscripts:

| | |
|---|---|
| $'$ | estimated value |

# APPENDIX B

## CORRELATION EQUATIONS

Correlation equations are developed whereby flow conditions ($U$, $V$, and $\psi/\psi_n$) within any impeller with straight blades can be determined from the flow conditions for the standard solution of this report.

### TANGENTIAL-VELOCITY RATIO $U$

A plot of $U$ against $\eta$ (equal to $\theta/\Delta\theta$, equation (10b)) at $\xi$ equal to 0 for various design and operating conditions (used in the relaxation solutions of this report) is shown in figure 18. These curves are representative examples of the variation in $U$ for all values of $\xi$ at which $U$ is significant. For a given value of $\xi$ and $\eta$, the tangential-velocity ratio $U$ is seen to be a function primarily of the impeller-tip Mach number $M_T$ and the angle between blades on the conic flow surface $\Delta\theta$. The tangential-velocity ratio is essentially independent of the compressor flow rate (flow coefficient $\varphi$) and the variation of passage-height ratio with $R$ (passage-height exponent $m$). This dependence of $U$ on $M_T$ and $\Delta\theta$ only (for a given value of $\xi$ and $\eta$) was found to exist at all radius ratios at which $U$ is significant and was found to be a direct relation such that

$$U=KM_T\Delta\theta$$

where $K$ is a function of $\xi$ and $\eta$ that is constant for all design and operating conditions. In terms of the standard solution, therefore,

$$U'=AU_s \tag{B1}$$

where

$$A=\frac{M_T\Delta\theta}{(M_T\Delta\theta)_s} \tag{B2}$$

and where the subscript $s$ refers to values from the standard example and the prime indicates the estimated value for the nonstandard example. Equation (B1) is the correlation equation for the relative tangential-velocity ratio.

The correlation equation (B1) and the other correlation equations to be developed in this appendix refer to the same transformed coordinates $\xi$ and $\eta$ for both the standard and nonstandard quantities in the equations. From equations (10a) and (10b), these transformed coordinates are related to the coordinates in the physical $(R,\theta)$ plane by

$$R=exp\ (\xi\Delta\theta) \tag{B3}$$

and

$$\theta=\eta\Delta\theta \tag{B4}$$

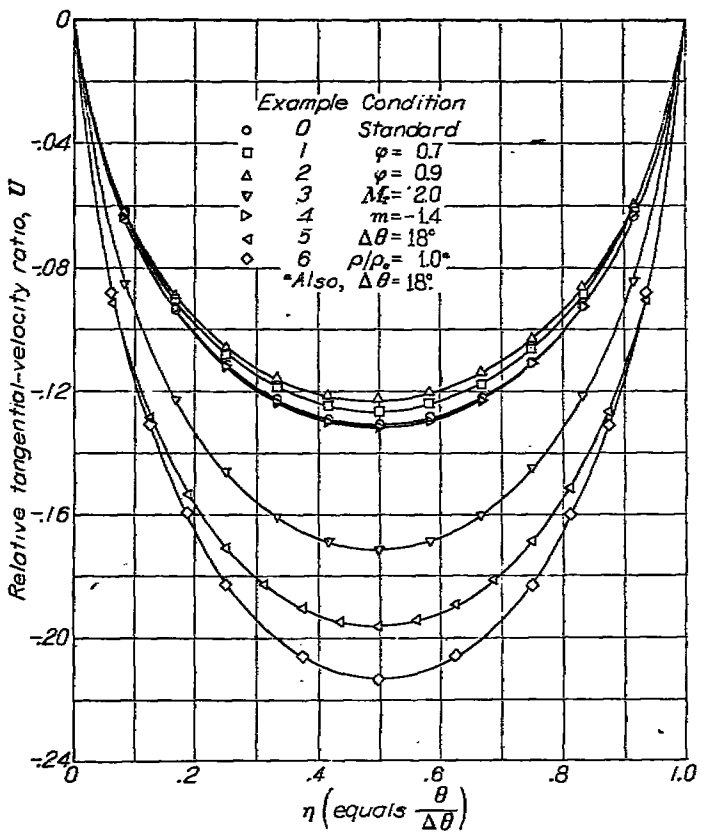


FIGURE 18.—Variation in relative tangential-velocity ratio across impeller passage for $\xi=0$. Plotted points obtained from relaxation solution.

### RADIAL-VELOCITY RATIO $V$

The correlation equation for the radial-velocity ratio is obtained from the equation for irrotational absolute motion of a fluid particle. From reference 1,

$$-2M_T=\frac{U}{R}+\frac{\partial U}{\partial R}-\frac{1}{R}\frac{\partial V}{\partial \theta}$$

which, after multiplying by $\Delta\theta$, becomes

$$-2M_T\Delta\theta=\left(\frac{U}{R}+\frac{\partial U}{\partial R}\right)\Delta\theta-\frac{1}{R}\frac{\partial V}{\partial \eta} \tag{B5}$$

Plots of $V$ against $\eta$ for various design and operating conditions and for $\xi$ equal to 0 and $-1.0$ are shown in figure 19. These plots are representative of the variation in $V$ at all values of $\xi$ within the impeller. The slopes of the velocity profiles $\frac{\partial V}{\partial \eta}$ are seen to be nearly constant (except in the immediate vicinity of the blade tip) so that from equation (B5)

$$\left(\frac{U}{R}+\frac{\partial U}{\partial R}\right)=f(\xi \text{ only}) \tag{B6}$$

and equation (B5) can be integrated to give

$$V=V_p+2RM_T(\Delta\theta)\eta+R(\Delta\theta)\left(\frac{U}{R}+\frac{\partial U}{\partial R}\right)\eta \tag{B7}$$

where $V$ equals $V_p$ and $\eta$ equals zero along the positive blade surface.

The velocity ratio $V_p$ can be evaluated from the condition

$$\left.\begin{aligned} V&=V_m \\ \eta&=\frac{\theta}{\Delta\theta}=0.5 \end{aligned}\right\} \tag{B8}$$

when

where $V_m$ is the mean radial-velocity ratio, which is obtained from continuity considerations as follows:

$$W=\rho_m V_m rhB\Delta\theta$$

or

$$\frac{W}{\rho_o a_T c_o}=\varphi=\frac{\rho_m}{\rho_o}V_m RH$$

so that

$$V_m=\frac{\varphi}{\frac{\rho_m}{\rho_o}RH} \tag{B9}$$

The mean density ratio $\rho_m/\rho_o$ in equation (B9) is obtained from equation (12) by assuming that for straight blades the relative tangential velocity is zero and the radial-velocity ratio is equal to the mean radial-velocity ratio $V_m$

$$Q^2\approx V_m{}^2=\left(\frac{\varphi}{\frac{\rho_m}{\rho_o}RH}\right)^2$$

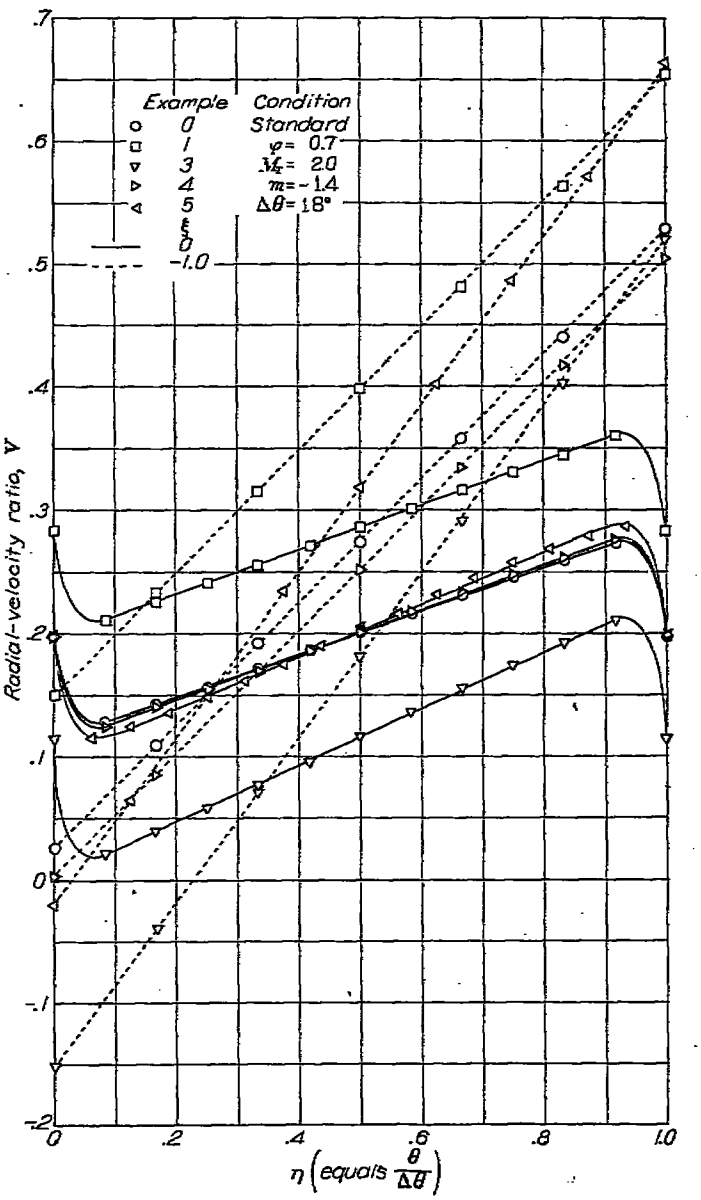


FIGURE 19.—Variation in radial-velocity ratio across impeller passage for two values of $\xi$. Plotted points obtained from relaxation solution.

Equation (12) becomes

$$\frac{\rho_m}{\rho_o}=\left\{1+\frac{\gamma-1}{2}\left[(RM_T)^2-\left(\frac{\varphi}{\frac{\rho_m}{\rho_o}RH}\right)^2\right]\right\}^{\frac{1}{\gamma-1}} \tag{B10}$$

Equation (B10) gives an average value of the density ratio, which is assumed to be a function of $\xi$ (that is, $(\log_e R)/\Delta\theta$) and independent of $\eta$ (that is, $\theta/\Delta\theta$).

From equation (B7) and the condition given by equation (B8), the velocity ratio $V_p$ becomes

$$V_p=V_m-RM_T\Delta\theta-\frac{R\Delta\theta}{2}\left(\frac{U}{R}+\frac{\partial U}{\partial R}\right)$$

and equation (B6) becomes

$$V=V_m+RM_T\Delta\theta(2\eta-1)+\frac{R\Delta\theta}{2}\left(\frac{U}{R}+\frac{\partial U}{\partial R}\right)(2\eta-1) \tag{B11}$$

From equation (B3),

$$\frac{\partial U}{\partial R}=\frac{\partial U}{\partial \xi}\frac{d\xi}{dR}=\frac{1}{R\Delta\theta}\frac{\partial U}{\partial \xi}$$

and from equation (B1),

$$\left(\frac{U}{R}+\frac{\partial U}{\partial R}\right)=\frac{A}{R\Delta\theta}\left(U_s\Delta\theta+\frac{\partial U_s}{\partial \xi}\right) \tag{B12}$$

so that equation (B11) becomes

$$V=V_m+RM_T\Delta\theta(2\eta-1)+\frac{A}{2}\left(U_s\Delta\theta+\frac{\partial U_s}{\partial \xi}\right)(2\eta-1)$$

which is solved for $\partial U_s/\partial\xi$

$$\frac{\partial U_s}{\partial \xi}=\frac{V-V_m}{\frac{A}{2}(2\eta-1)}-\frac{2RM_T\Delta\theta}{A}-U_s\Delta\theta$$

The term $\partial U_s/\partial\xi$ can be eliminated by equating it for the standard and nonstandard cases. Therefore,

$$V'=V_m+A(V-V_m)_s+$$
$$A(2\eta-1)\left\{\frac{U_s}{2}[\Delta\theta-(\Delta\theta)_s]+(R-R_s)(M_T\Delta\theta)_s\right\} \tag{B13}$$

Equation (B13) is the correlation equation for the radial-velocity ratio.

### STREAM-FUNCTION RATIO $\psi/\psi_n$

The stream-function ratio is obtained from the definition of the stream function and from the correlation equation for the radial-velocity ratio $V$. The definition of the stream function is given by equation (4a):

$$\frac{\partial\psi}{\partial\theta}=\frac{\rho}{\rho_o}VHR \tag{4a}$$

which, after being multiplied by $\Delta\theta$ and combined with equation (B11), becomes

$$\frac{\partial\psi}{\partial\eta}=\frac{\rho}{\rho_o}RH(\Delta\theta)\left[V_m+RM_T(\Delta\theta)(2\eta-1)+\frac{R\Delta\theta}{2}\left(\frac{U}{R}+\frac{\partial U}{\partial R}\right)(2\eta-1)\right] \tag{B14}$$

From the condition given by equation (B6) and with the density ratio replaced by its mean value for $\xi$ (that is, $(\log_e R)/\Delta\theta$), equation (B14) can be integrated to give

$$\frac{\psi}{\psi_n}=\frac{1}{V_m}\left[V_m+RM_T(\Delta\theta)(\eta-1)+\frac{R\Delta\theta}{2}\left(\frac{U}{R}+\frac{\partial U}{\partial R}\right)(\eta-1)\right]\eta \tag{B15}$$

where $\psi_n$ is given by equation (5) and $\psi/\psi_n$ is equal to zero when $\eta$ is equal to zero. Introducing equation (B12) and solving for $\partial U_s/\partial\xi$ give

$$\frac{\partial U_s}{\partial\xi}=\frac{V_m\left(\frac{\psi}{\psi_n}-\eta\right)-RM_T(\Delta\theta)(\eta-1)\eta}{\frac{A}{2}(\eta-1)\eta}-U_s\Delta\theta$$

The term $\partial U_s/\partial\xi$ can be eliminated by equating it for the standard and nonstandard cases; therefore

$$\frac{\psi'}{\psi_n}=\eta+\frac{A}{V_m}\left(\left[V_m\left(\frac{\psi}{\psi_n}-\eta\right)\right]_s+\right.$$
$$\left.\eta(\eta-1)\left\{\frac{U_s}{2}[\Delta\theta-(\Delta\theta)_s]+(R-R_s)(M_T\Delta\theta)_s\right\}\right) \tag{B16}$$

Equation (B16) is the correlation equation for the stream-function ratio.

## APPENDIX C

### CORRELATION EQUATION FOR IMPELLER SLIP FACTOR

The impeller slip factor is defined as the ratio of the average absolute tangential velocity of the fluid leaving the impeller tip to the tip speed of the impeller. This definition results in the following equation (reference 1):

$$\mu=1+\frac{U_m}{M_T} \tag{C1}$$

Also, from equations (B1) and (B2)

$$\frac{U_{m'}}{M_T}=\left(\frac{U_m}{M_T}\right)_s\frac{\Delta\theta}{(\Delta\theta)_s}$$

which, from equation (C1), becomes

$$\mu'-1=(\mu_s-1)\frac{\Delta\theta}{(\Delta\theta)_s}$$

or

$$\mu'=1-(1-\mu_s)\frac{\Delta\theta}{(\Delta\theta)_s} \tag{C2}$$

Equation (C2) is the correlation equation for the slip factor.

### REFERENCES

1. Stanitz, John D.: Two-Dimensional Compressible Flow in Turbomachines with Conic Flow Surfaces. NACA Rep. 935, 1949.
2. Emmons, Howard W.: The Numerical Solution of Compressible Fluid Flow Problems. NACA TN 932, 1944.

## TABLE I—STREAM-FUNCTION RATIO $\psi/\psi_n$ FOR STANDARD SOLUTION

[Conditions for standard example: $(\varphi)_s=0.5$; $(M_T)_s=1.5$; $(m)_s=-1.0$; $(\Delta\theta)_s=0.20944$ radian; $(\gamma)_s=1.4$]

| $(V_m)_s$ | $R_s$ | $\xi$ | $\eta$ (equals $\theta/\Delta\theta$) | | | | | | | | | | |
|---|---|---|---|---|---|---|---|---|---|---|---|---|---|
| | | | 0 | 0.1 | 0.2 | 0.3 | 0.4 | 0.5 | 0.6 | 0.7 | 0.8 | 0.9 | 1.0 |
| 0.3168 | 0.70 | −1.7030 | 0 | 0.040 | 0.095 | 0.165 | 0.244 | 0.341 | 0.451 | 0.570 | 0.702 | 0.848 | 1.000 |
| .2941 | .75 | −1.3736 | 0 | .031 | .078 | .143 | .220 | .316 | .427 | .549 | .656 | .840 | 1.000 |
| .2735 | .80 | −1.0654 | 0 | .022 | .061 | .120 | .197 | .291 | .401 | .529 | .671 | .831 | 1.000 |
| .2536 | .85 | −.7760 | 0 | .014 | .047 | .101 | .177 | .270 | .383 | .509 | .655 | .824 | 1.000 |
| .2348 | .90 | −.5031 | 0 | .011 | .042 | .097 | .171 | .255 | .377 | .503 | .650 | .819 | 1.000 |
| .2275 | .92 | −.3981 | 0 | .012 | .046 | .102 | .177 | .270 | .382 | .506 | .651 | .816 | 1.000 |
| .2202 | .94 | −.2954 | 0 | .016 | .054 | .113 | .189 | .283 | .392 | .517 | .660 | .820 | 1.000 |
| .2133 | .96 | −.1949 | 0 | .023 | .069 | .132 | .212 | .305 | .413 | .536 | .675 | .828 | 1.000 |
| .2100 | .97 | −.1454 | 0 | .029 | .080 | .146 | .228 | .321 | .429 | .550 | .684 | .832 | 1.000 |
| .2067 | .98 | −.0965 | 0 | .038 | .093 | .163 | .247 | .341 | .447 | .566 | .697 | .839 | 1.000 |
| .2034 | .99 | −.0480 | 0 | .048 | .111 | .185 | .270 | .366 | .472 | .586 | .713 | .850 | 1.000 |
| .2002 | 1.00 | 0 | 0 | .062 | .133 | .210 | .297 | .393 | .499 | .611 | .734 | .862 | 1.000 |

## TABLE II—RADIAL-VELOCITY RATIO $V$ FOR STANDARD SOLUTION

[Conditions for standard example: $(\varphi)_s=0.5$; $(M_T)_s=1.5$; $(m)_s=-1.0$; $(\Delta\theta)_s=0.20944$ radian; $(\gamma)_s=1.4$]

| $(V_m)_s$ | $R_s$ | $\xi$ | $\eta$ (equals $\theta/\Delta\theta$) | | | | | | | | | | |
|---|---|---|---|---|---|---|---|---|---|---|---|---|---|
| | | | 0 | 0.1 | 0.2 | 0.3 | 0.4 | 0.5 | 0.6 | 0.7 | 0.8 | 0.9 | 1.0 |
| 0.3163 | 0.70 | −1.7030 | 0.103 | 0.146 | 0.190 | 0.234 | 0.278 | 0.323 | 0.368 | 0.412 | 0.456 | 0.501 | 0.549 |
| .2941 | .75 | −1.3736 | .065 | .112 | .159 | .206 | .253 | .301 | .345 | .396 | .443 | .492 | .543 |
| .2735 | .80 | −1.0654 | .033 | .082 | .132 | .181 | .230 | .280 | .329 | .378 | .428 | .479 | .533 |
| .2536 | .85 | −.7760 | .008 | .059 | .110 | .160 | .210 | .259 | .309 | .357 | .408 | .460 | .515 |
| .2348 | .90 | −.5031 | −.001 | .049 | .099 | .148 | .194 | .239 | .285 | .330 | .378 | .430 | .483 |
| .2275 | .92 | −.3981 | .002 | .051 | .100 | .146 | .189 | .231 | .273 | .316 | .363 | .413 | .463 |
| .2202 | .94 | −.2954 | .010 | .058 | .105 | .148 | .186 | .224 | .261 | .299 | .342 | .390 | .438 |
| .2133 | .96 | −.1949 | .025 | .072 | .115 | .161 | .184 | .216 | .248 | .280 | .316 | .360 | .407 |
| .2100 | .97 | −.1454 | .037 | .082 | .122 | .155 | .184 | .213 | .241 | .270 | .301 | .342 | .388 |
| .2067 | .98 | −.0965 | .055 | .095 | .131 | .158 | .184 | .209 | .234 | .259 | .286 | .321 | .362 |
| .2034 | .99 | −.0480 | .091 | .115 | .139 | .161 | .184 | .205 | .227 | .249 | .271 | .293 | .316 |
| .2002 | 1.00 | 0 | .199 | .131 | .148 | .166 | .184 | .202 | .220 | .238 | .254 | .271 | .199 |

## TABLE III—RELATIVE TANGENTIAL-VELOCITY RATIO $U$ FOR STANDARD SOLUTION

[Conditions for standard example: $(M_T)_s=1.5$; $(\Delta\theta)_s=0.20944$ radian]

| $R_s$ | $\xi$ | $\eta$ (equals $\theta/\Delta\theta$) | | | | | | | | | | |
|---|---|---|---|---|---|---|---|---|---|---|---|---|
| | | 0 | 0.1 | 0.2 | 0.3 | 0.4 | 0.5 | 0.6 | 0.7 | 0.8 | 0.9 | 1.0 |
| 0.70 | −1.7030 | 0 | 0.008 | 0.015 | 0.020 | 0.023 | 0.024 | 0.023 | 0.020 | 0.015 | 0.008 | 0 |
| .75 | −1.3736 | 0 | .008 | .015 | .020 | .023 | .024 | .023 | .020 | .015 | .008 | 0 |
| .80 | −1.0654 | 0 | .008 | .014 | .018 | .021 | .022 | .021 | .019 | .015 | .008 | 0 |
| .85 | −.7760 | 0 | .005 | .009 | .011 | .012 | .013 | .013 | .012 | .010 | .006 | 0 |
| .90 | −.5031 | 0 | −.002 | −.004 | −.007 | −.008 | −.008 | −.007 | −.005 | −.003 | −.001 | 0 |
| .92 | −.3981 | 0 | −.007 | −.013 | −.018 | −.021 | −.022 | −.021 | −.016 | −.011 | −.005 | 0 |
| .94 | −.2954 | 0 | −.013 | −.024 | −.033 | −.038 | −.039 | −.037 | −.031 | −.022 | −.012 | 0 |
| .96 | −.1949 | 0 | −.023 | −.041 | −.054 | −.061 | −.063 | −.060 | −.052 | −.039 | −.021 | 0 |
| .97 | −.1454 | 0 | −.030 | −.053 | −.068 | −.076 | −.077 | −.074 | −.066 | −.050 | −.029 | 0 |
| .98 | −.0965 | 0 | −.040 | −.067 | −.083 | −.091 | −.094 | −.091 | −.081 | −.065 | −.039 | 0 |
| .99 | −.0480 | 0 | −.053 | −.083 | −.100 | −.109 | −.112 | −.108 | −.099 | −.082 | −.052 | 0 |
| 1.00 | 0 | 0 | −.072 | −.102 | −.119 | −.126 | −.131 | −.127 | −.118 | −.100 | −.070 | 0 |